The Weierstrass Drift: A Toy SLE Brownian Model

Claire David, Michel Lapidus

The Weierstrass Drift: A Toy SLE Brownian Model

Claire David [1] [*] **and Michel L. Lapidus** [2] [†]

April 29, 2026

[1] Sorbonne Université
CNRS, UMR 7598, Laboratoire Jacques-Louis Lions, 4, place Jussieu 75005, Paris, France

[2] University of California, Riverside, Department of Mathematics,
Skye Hall, 900 University Ave., Riverside, CA 92521-0135, USA

Abstract

We revisit the use of the Weierstrass function as a deterministic driving term for the Loewner equation, in connection with the Schramm–Loewner evolution (SLE), a setting first considered by Joan Lind and Jessica Robbins in [LR17].

Building on this idea, we study Loewner evolutions driven by a Weierstrass drift and obtain explicit and sharp estimates for the $\mathrm{Lip}(\delta)$ norm of the Weierstrass function. These estimates are valid for all $\delta \in (0, \frac{1}{2}]$ and significantly improve the classical $\mathrm{Lip}(\frac{1}{2})$ bounds obtained in [LR17] via truncation methods.

As a consequence, we derive refined quantitative bounds for the critical scaling parameter multiplying the driving term that separates regimes where the corresponding Loewner traces are simple curves from those where self-intersections occur.

We further compare the dynamics generated by truncated and prefractal approximations of the Weierstrass function. Our results indicate that prefractal drifts more faithfully capture the multiscale roughness and geometric complexity associated with Brownian-driven SLE. This provides a natural deterministic framework for investigating geometric transitions and multifractal features in Loewner evolutions driven by rough signals.

MSC Classification: 28A75-28A80-30C35-35R02-57Q70.

Keywords: Schramm–Loewner equation, SLE, drift, Brownian motion, $\mathrm{Lip}\left(\frac{1}{2}\right)$ norm, $\mathrm{Lip}\,(\delta)$ norm,Weierstrass function and curve.

[*]This project has received financial support from the CNRS via the MITI interdisciplinary programs through its exploratory research program. The research of C. D.and M. L. L. is supported by the MITI CNRS 80PRIME, Conditions Extrêmes, Formes Optimales and by the ANR FRACTALS (ANR-24-CE45-3362).

[†]The research of M. L. L. was supported by the Burton Jones Endowed Chair in Pure Mathematics, as well as by grants from the U. S. National Science Foundation.

Contents

1 Introduction

As is explained in [RS05], Schramm–Loewner evolution (in short, SLE) [Sch00] is "a random process of growth of a set K_t" (the so-called SLE *hull*), in connection with the one-dimensional Brownian motion, which plays the role of "a drift" – also often called *the driving term*, governing the evolution of the set under study. More precisely, given $T > 0$, along with a continuous, real-valued function Λ, defined on $[0,T]$, we are interested in the solution $g : [0,T] \times \mathbb{H} \to \mathbb{C}$ of the chordal backward Loewner (partial) differential equation (in short, Loewner equation),

$$\forall\, (t,z) \in [0,T] \times \mathbb{H} : \quad \frac{\partial g}{\partial t} = -\frac{2}{g(t,z) - \Lambda(t)} \qquad (\mathcal{L})$$

with the initial condition $g(t_0, z) = z$.

The sets of singularities associated with the SLE [Sch00], in the case of a Brownian motion drift $t \mapsto \sqrt{\kappa}\, B(t)$, where $t \mapsto B(t)$ is the Brownian motion, and κ is a strictly positive constant, consist of curves which – depending on the value of the parameter κ – can be fractal – the so-called SLE_κ traces (in short, SLE_κ); see, in particular, the discussion at the beginning of Section 3. As is explained by Bertrand Duplantier in [Dup89], [DB08], those (conformally invariant) fractal curves appear in critical phenomena which arise in statistical systems (critical Ising or Potts percolation clusters, in the case of ferromagnets and the associated atomic spins, for instance). They can be associated with *phase transitions* – the Potts model, which is a variant of the Ising model, is often used to study phase transitions. For the reader interested in classical references on probability theory and fractals, random fractals, diffusions on fractals, percolation and the SLE process, we refer to the introduction of the book [LR25] by the second author and Goran Radunović, and, more specifically, to the books of Christopher J. Bishop and Yuval Peres [BP17], Peter Mörters and Yuval Peres [MP10], along with the book by Gregory F. Lawler entitled *Conformally Invariant Processes in the Plane* [Law05], as well as to the papers by Stanislav Smirnov and Wendelin Werner in [SW01], by Wendelin Werner, Gregory F. Lawler and Oded Schramm in [LSW01], by Wendelin Werner in [Wer04], on random planar curves and Schramm–Loewner evolutions; see also the survey articles by Martin T. Barlow [Bar98], by Bertrand Duplantier in [Dup04], by Bertrand Duplantier, Rémi Rhodes, Scott Sheffield and Vincent Vargas in [DRSV17], on *Log-correlated Gaussian fields: An overview*, as well as by Jean-François Le Gall in [LG14], [LG19], on Random geometry on the sphere and on Brownian geometry, respectively.

The Weierstrass function, which stands as the deterministic analog of the Brownian motion in terms of roughness and Hölder regularity, can be used in order to study SLE_κ traces. Let us recall a

few facts about the Weierstrass function $\mathcal{W}$, which is a celebrated example of a continuous but nowhere differentiable function, and the associated Weierstrass Curve (the graph of $\mathcal{W}$). Given $\lambda \in]0,1[$, and b such that $\lambda\, b > 1 + \dfrac{3\,\pi}{2}$, the Weierstrass function is defined as the sum of the uniformly convergent trigonometric series

$$x \in \mathbb{R} \mapsto \mathcal{W}(x) = \sum_{n=0}^{\infty} \lambda^n \cos\left(2\,\pi\, b^n\, x\right) .$$

The original proof (of the nowhere differentiability of $\mathcal{W}$), by K. Weierstrass [Wei75], in the case where b is an odd positive integer, can also be found in [Tit39] (pages 351-353). It has been completed by the one, now classical, given by G. H. Hardy [Har16], in the more general case, where b is any real number such that $\lambda\, b > 1$.

In the case where $b = N_b \geqslant 3$ is an integer, the authors of the present paper have obtained the exact values of the local extrema. They have also determined the optimal Hölder exponent of the Weierstrass function $\mathcal{W}$. Those extrema – which form a dense subset of the Weierstrass Curve – directly depend on the choice of an initial set of points, which happen to be here the fixed points of the nonlinear iterated function system involved in the construction of the Curve; see [Dav19] for further details.

Back to the SLE_κ context, one of the main questions is the nature of the traces, and, consequently, the thresholds associated with phase transitions, from simple paths ($0 \leqslant \kappa \leqslant 4$, nonsimple paths ($4 < \kappa < 8$) and space-filling curves ($\kappa \geqslant 8$; see the paper by Oded Schramm and Steffen Rohde [RS05], where they prove this result. They also conjectured a connection between the fractal nature of the traces (in terms of their Hausdorff dimension) and the value of κ. It was later proved by Vincent Beffara in [Bef08] that the value of the Hausdorff dimension of the trace was almost surely equal to $\min\left(2, 1 + \dfrac{\kappa}{8}\right)$.

Along these lines, in [**?**], Oded Schramm and Steffen Rohde asked whether there existed an analogous classification in the deterministic setting, i.e., when the driving term in SLE is an analytic function Λ. By relying on the notions of *slit half-plane*, namely, any plane domain of the form $\mathbb{H} \setminus \gamma$, where $\gamma : [0,1] \to \mathbb{H} \cup \gamma(0)$ denotes a simple curve of $\mathbb{H} \cup \gamma(0)$, and of *quasi-slit half-plane*, namely, the image of $\mathbb{H} \setminus [0,i]$ under a quasiconformal mapping fixing $\mathbb{H}$ and ∞, they proved the existence of a positive and finite constant C_0 such that if the $\mathrm{Lip}\left(\dfrac{1}{2}\right) = \sup\limits_{x \in \mathbb{R}} \sup\limits_{h>0} \dfrac{|\Lambda(x+h) - \Lambda(x)|}{h^{\frac{1}{2}}}$ norm of the driving function Λ is smaller than C_0, the domains generated by Λ (in the sense of the traces of SLE_κ in the plane) are quasi-slit half-planes.

Based upon this result, Joan Lind obtained in [Lin05] the explicit upper bound 4 for the constant C_0.

In their seminal paper [LR17], Joan Lind and Jessica Robbins then investigated the traces of SLE_κ in the case where the drift Λ is collinear with the Weierstrass function. They showed that, as is the case in the usual Schramm–Loewner equation (i.e., when the drift is the Brownian motion), there is *a phase transition*, corresponding to the fact that the traces can be simple or non-simple curves. For this purpose, they required the value of the $\mathrm{Lip}\left(\dfrac{1}{2}\right)$ norm of the Weierstrass function, which is obtained by truncation. The authors of [LR17] acknowledge that the theoretical bounds they provide are not optimal, in the light of their numerical experimental data, associated with the computation of sets of values of the Weierstrass function. If they obtain a universal threshold, they do not capture the fine structure of deterministic fractal (Weierstrass) drifts, which require sharper estimates.

The purpose of the present paper is to study Loewner evolutions driven by deterministic fractal signals, using the Weierstrass function as a canonical example. By obtaining explicit estimates for the Lip(δ) norm of the Weierstrass function, we derive refined bounds for the scaling parameter governing the transition between simple and non-simple Loewner traces. These estimates improve the truncation-based bounds obtained by Lind and Robbins in [LR17].

Building on our previous analysis of the Weierstrass function [DL25d], [DL24c], [DL24a], [DL25a], [DL24b], [DL25b], [DL25c], we obtain more general results, namely, for $\delta \in \left]0, \frac{1}{2}\right]$, bounds for the Lip (δ) norm of the Weierstrass function and, for $\delta = \frac{1}{2}$, improved bounds compared with those obtained by J. Lind and J. Robbins in [LR17]. In contrast with the truncation approach of Lind and Robbins, our method exploits the exact values of the Weierstrass function at its local extrema, which allows us to derive sharp estimates for the Lip (δ) norm and significantly narrow the gap between the theoretical bounds governing the phase transition. Our results are all the more important, insofar as they enable us to more precisely determine the range of values of the real parameter c such that the Weierstrass drift $c\,\widetilde{W}$ shows a phase transition (corresponding to Loewner traces as simple or multiple curves). We also obtain the results associated with the less restrictive general case of a Lip (δ) drift, with $0 < \delta \leqslant \frac{1}{2}$, a configuration all the more interesting, insofar as the Brownian motion is almost surely Hölder continuous with associated Hölder exponent $\delta \in \left]0, \frac{1}{2}\right[$, or, more precisely, with $\delta = \frac{1}{2} - \varepsilon$, for an arbitrarily small $\varepsilon > 0$. Our deterministic Weierstrass framework could, therefore, provide a better understanding of the singularities of multifractal SLE traces.

It so happens that the method developed in [DL25d], [DL24c], [DL24a], [DL25a], [DL24b], [DL25b], [DL25c], can also be applied in the case $N_b = 2$ – which corresponds to what can be found in [LR17]. Note that due to the one-periodicity of the Weierstrass function (since N_b is an integer), we have restricted our study to the half-open unit interval $[0, 1[= [0, 1)$. In [LR17], the authors work with the equivalent $2\,\pi$-periodic expression, given, for all $t \in \mathbb{R}$, by (with our notation for $\mathcal{W}$ introduced in relations $(\mathcal{R}1)$ and $(\mathcal{R}3)$ below)

$$\widetilde{\mathcal{W}}(t) = \mathcal{W}\left(\frac{t}{2\,\pi}\right) = \sum_{n=0}^{\infty} \lambda^n \, \cos\left(N_b^n \, t\right) \, .$$

Our results, which are simply the extension to the case $N_b \geqslant 2$ of our previous works (where $N_b \geqslant 3$), enable us to obtain the (better) sought for bounds, and, hence, the exact threshold for the transition from simple to non-simple Loewner traces. This result comes from the fact that our bounds are better than the ones obtained in [LR17]. More precisely, in [LR17], the authors work with the infinite series expression of the Weierstrass function, which they truncate. In addition, they do not have at their disposal the exact values taken by the Weierstrass function at its local extrema, which we have obtained in our previous works [DL25d], [DL25b]; see Corollary 2.7 below. Along these lines, we have at our disposal the exact values of the Weierstrass function for a dense subset of the unit interval, which enables us to obtain better estimates. The model we develop therefore fundamentally differs from the approach in [LR17], insofar as it provides explicit sharpLip (δ) bounds and exact phase-transition thresholds, which were not accessible with the truncation approach used in the aforementioned work.

The details of our method are provided in Section 2. Our main result, for the Lip (δ) norm of the Weierstrass function – the deterministic counterpart of the parameter κ – where $0 < \delta \leqslant \frac{1}{2}$, is Theorem 2.8. The resulting optimal bounds associated with the *phase transition*, when $\delta = \frac{1}{2}$, are displayed in Table 3.

We then raise the question, in Section 3, of the possible connections with the trace of SLE_κ and generalized Weierstrass functions, still in the case of a Weierstrass drift, by using the notion of *quasi-self similarity* introduced in [DL25b], or, also, the *self-shape similarity* of the patterns that arise on the traces; see [DL25d]. Note that we go much further than what is done in [LR17], since we conduct a comparative study, in the case of Weierstrass-prefractal driven hulls – when the drift is a (piecewise linear) Weierstrass-prefractal function, corresponding to a realistic approximation of the Weierstrass function, which enables us to take into account its roughness – and in the case of Weierstrass-truncated driven hulls – when the drift is a sharp truncation of the Weierstrass function, by nature a smooth function, as is done in [LR17]. By computing the associated Chhabra–Jensen multifractal spectra, we are finally able to show that the polygonal depth of the drift controls the appearance of new scales both in the drift and in the resulting hull, which highlights a fundamental connection between the regularity of the drift and the geometric complexity of the trace: small-scale oscillations of the driving function induce corresponding geometric oscillations of the hull.

2 Lip (δ) Norm of the Weierstrass Function

Henceforth, we place ourselves in the Euclidean plane, equipped with a direct orthonormal frame. The usual Cartesian coordinates are denoted by (x, y). The horizontal and vertical axes will be respectively referred to as (Ox) and (Oy).

Notation 1 (**Weierstrass Parameters [DL25d]**).

In the sequel, λ and N_b are two real numbers such that

$$0 < \lambda < 1 \quad , \quad N_b \in \mathbb{N}^\star \quad \text{and} \quad \lambda\, N_b > 1\,. \tag{$\mathcal{R}$ 1}$$

As explained in [Dav19], we deliberately made the choice to introduce the notation N_b which replaces the initial b, in so far as, in Hardy's paper [Har16] (in contrast to Weierstrass's original article [Wei75]), b is any positive real number satisfying $\lambda\, b > 1$, whereas we deal here with the specific case of a positive integer, which accounts for the natural notation N_b.

In the sequel, we will work with $N_b \geqslant 2$. We also keep λ as a parameter, which will enable us to obtain more general results than in [LR17]. In the end, we will, of course, consider the value $\lambda = \dfrac{1}{\sqrt{2}}$, as in [LR17].

Definition 2.1 (**Weierstrass Function, Weierstrass Curve [DL25d]**).

We consider the *Weierstrass function* $\mathcal{W}$, defined, for any real number x, by

$$\mathcal{W}(x) = \sum_{n=0}^{\infty} \lambda^n \cos\left(2\,\pi\, N_b^n\, x\right)\,. \tag{$\mathcal{R}$ 2}$$

We call the associated graph the *Weierstrass Curve*.

Due to the one-periodicity of the $\mathcal{W}$-function (since N_b is an integer), from now on, and without loss of generality, we restrict our study to the interval $[0,1[\,=[0,1)$.

For the sake of comparison with the results in [LR17], we also introduce *the (equivalent)* $2\,\pi$*-periodic Weierstrass function*, defined, for any real number t, by

$$\widetilde{\mathcal{W}}(t) = \mathcal{W}\left(\frac{t}{2\,\pi}\right) = \sum_{n=0}^{\infty} \lambda^n \,\cos\left(N_b^n\, t\right)\,. \tag{$\mathcal{R}\,3$}$$

Notation 2. For the parameters λ and N_b satisfying condition ($\mathcal{R}1$) (see Notation 1, on page 5), we denote by

$$D_{\mathcal{W}} = 2 + \frac{\ln\lambda}{\ln N_b} = 2 - \ln_{N_b}\frac{1}{\lambda} \;\in\;]1,2[\tag{$\mathcal{R}\,4$}$$

the box-counting dimension (or Minkowski dimension) of the Weierstrass Curve $\Gamma_{\mathcal{W}}$, which happens to be equal to the Hausdorff dimension of $\Gamma_{\mathcal{W}}$ [KMPY84], [BBR14], [She18], [Kel17]. As was mentioned earlier, our methods and results in [DL25b] and [DL25a] also provide a direct geometric proof of the fact that $D_{\mathcal{W}}$, the Minkowski dimension (or box-counting dimension) of $\Gamma_{\mathcal{W}}$, exists and takes the above value; see [DL25b], Theorem 6. 1 in Section 6.

Proposition 2.1 (**Nonlinear and Noncontractive Iterated Function System (IFS) [DL25d]**)**.**

Following our previous work [Dav18]*, we approximate the restriction* $\Gamma_{\mathcal{W}}$ *to* $[0,1[\times\mathbb{R}$*, of the Weierstrass Curve, by a sequence of graphs, built via an iterative process. For this purpose, we use the nonlinear iterated function system (IFS) consisting of the family of* C^∞ *maps from* $\mathbb{R}^2$ *to* $\mathbb{R}^2$ *denoted by*

$$\mathcal{T}_{\mathcal{W}} = \left\{T_0, \ldots, T_{N_b-1}\right\}\,,$$

where, for any integer i *belonging to* $\{0,\ldots,N_b-1\}$ *and any point* (x,y) *of* $\mathbb{R}^2$*,*

$$T_i(x,y) = \left(\frac{x+i}{N_b}, \lambda\, y + \cos\left(2\,\pi\,\left(\frac{x+i}{N_b}\right)\right)\right)\,.$$

Then, $\Gamma_{\mathcal{W}}$ *is the unique attractor of the (noncontractive) IFS* $\mathcal{T}_{\mathcal{W}}$*; i.e., it is the unique nonempty compact subset* $\mathcal{L}$ *of* $\mathbb{R}^2$ *such that*

$$\mathcal{L} = \bigcup_{i=0}^{N_b-1} T_i\left(\mathcal{L}\right)\,.$$

Lemma 2.2. *For any integer* i *belonging to* $\{0,\ldots,N_b-1\}$*, the map* T_i *is a bijection from the graph* $\Gamma_{\mathcal{W}}$ *of the Weierstrass function onto* $\Gamma_{\mathcal{W}}$*.*

Proof. Let us consider $i \in \{0,\ldots,N_b-1\}$.

Consider a point $(y, \mathcal{W}(y))$ of $\Gamma_{\mathcal{W}}$, and let us look for a real number x of $[0,1]$ such that

$$T_i\,(x, \mathcal{W}(x)) = (y, \mathcal{W}(y))\ .$$

We then have that

$$x = 2\,y - i\,.$$

This enables one to obtain

$$\mathcal{W}(x) = \mathcal{W}(N_b\,y - i) = \sum_{n=0}^{+\infty} \lambda^n\ \cos\left(2\,\pi\,N_b^{n+1}\,y - 2\,\pi\,N_b^n\,i\right) = \sum_{n=0}^{+\infty} \lambda^n\ \cos\left(2\,\pi\,N_b^{n+1}\,y\right)$$

and

$$\begin{aligned} T_i\,(x, \mathcal{W}(x)) &= \left(\frac{x+i}{2}, \lambda\,\mathcal{W}(x) + \cos\left(2\,\pi\,\left(\frac{x+i}{2}\right)\right)\right) \\ &= \left(y, \sum_{n=0}^{+\infty} \lambda^{n+1}\ \cos\left(2\,\pi\,N_b^{n+1}\,y\right) + \cos\left(2\,\pi\,y\right)\right) \\ &= \left(y, \sum_{n=0}^{+\infty} \lambda^n\ \cos\left(2\,\pi\,N_b^n\,y\right)\right) \\ &= (y, \mathcal{W}(y))\ . \end{aligned}$$

Therefore, there exists a unique real number x such that

$$T_i\,(x, \mathcal{W}(x)) = (y, \mathcal{W}(y))\ .$$

By the one-periodicity of the Weierstrass function $\mathcal{W}$, we may assume, without loss of generality, that $x \in [0,1]$, as claimed.

□

Definition 2.2 (**Fixed Points [DL25d]**).

For any integer i belonging to $\{0, \ldots, N_b - 1\}$, we denote by

$$P_i = (x_i, y_i) = \left(\frac{i}{N_b - 1}, \frac{1}{1-\lambda}\ \cos\left(\frac{2\,\pi\,i}{N_b - 1}\right)\right)$$

the unique fixed point of the map T_i (see [Dav19]).

Definition 2.3 (**Sets of Vertices, Prefractals [DL25d]**).

We denote by V_0 the ordered set (according to increasing abscissae), of the points

$$\left\{P_0, \ldots, P_{N_b - 1}\right\}\ .$$

The set of points V_0 – where, for any i of $\{0, \ldots, N_b - 2\}$, the point P_i is linked to the point P_{i+1} – constitutes an oriented finite graph, ordered according to increasing abscissae, which we will denote by Γ_0. Then, V_0 is called *the set of vertices* of the graph Γ_0.

For any positive integer m, i.e., for $m \in \mathbb{N}^{\star}$, we set $V_m = \bigcup_{i=0}^{N_b-1} T_i\,(V_{m-1})$.

The set of points V_m, where two consecutive points are linked, is an oriented finite graph, ordered according to increasing abscissae, which we will call the $\boldsymbol{m^{th}}$ **order $\mathcal{W}$-prefractal** (or m^{th} prefractal graph approximation). Then, V_m is called *the set of vertices* of the prefractal Γ_m; see Figures 1,on page 9, and 2, on page 10, along with Figures 3, on page 12.

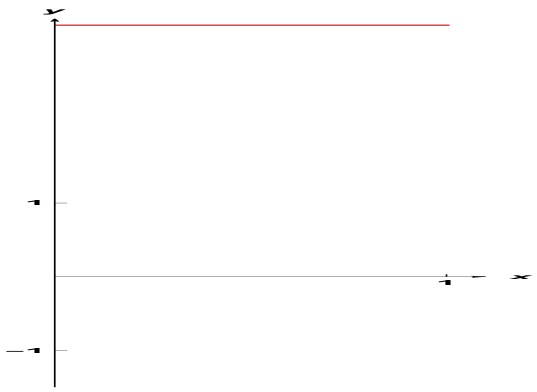

(a) **The prefractal graph $\Gamma_{\mathcal{W}_0}$, in the case when $\lambda = \frac{1}{\sqrt{2}}$ and $N_b = 2$.**

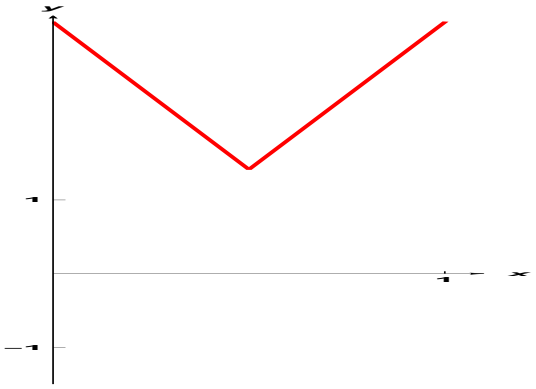

(b) **The prefractal graph $\Gamma_{\mathcal{W}_1}$, in the case when $\lambda = \frac{1}{\sqrt{2}}$ and $N_b = 2$.**

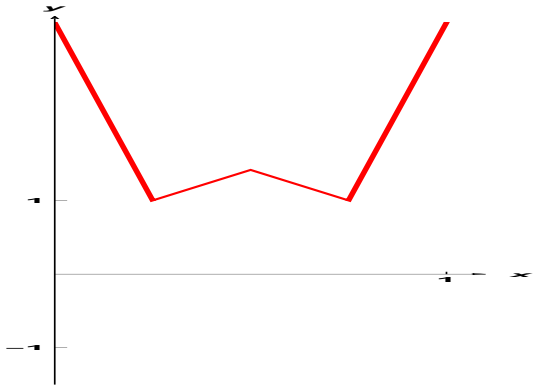

(c) **The prefractal graph $\Gamma_{\mathcal{W}_2}$, in the case when $\lambda = \frac{1}{\sqrt{2}}$ and $N_b = 2$.**

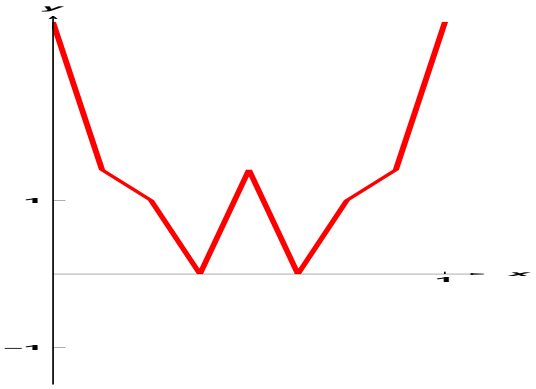

(d) **The prefractal graph $\Gamma_{\mathcal{W}_3}$, in the case when $\lambda = \frac{1}{\sqrt{2}}$ and $N_b = 2$.**

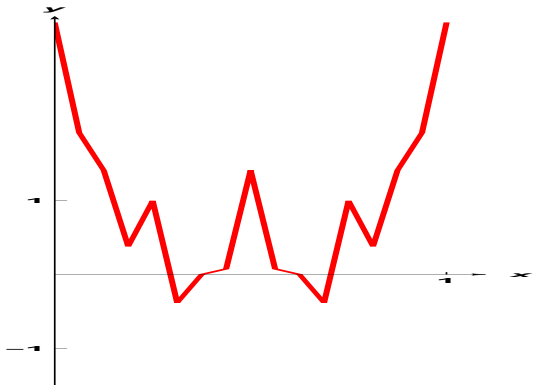

(e) **The prefractal graph $\Gamma_{\mathcal{W}_4}$, in the case when $\lambda = \frac{1}{\sqrt{2}}$ and $N_b = 2$.**

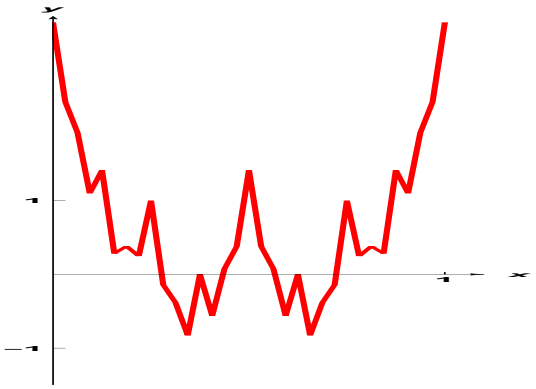

(f) **The prefractal graph $\Gamma_{\mathcal{W}_5}$, in the case when $\lambda = \frac{1}{\sqrt{2}}$ and $N_b = 2$.**

Figure 1: **The prefractal graphs $\Gamma_{\mathcal{W}_0}$, $\Gamma_{\mathcal{W}_1}$, $\Gamma_{\mathcal{W}_2}$, $\Gamma_{\mathcal{W}_3}$, $\Gamma_{\mathcal{W}_4}$, $\Gamma_{\mathcal{W}_5}$, in the case when $\lambda = \frac{1}{\sqrt{2}}$ and $N_b = 2$.**

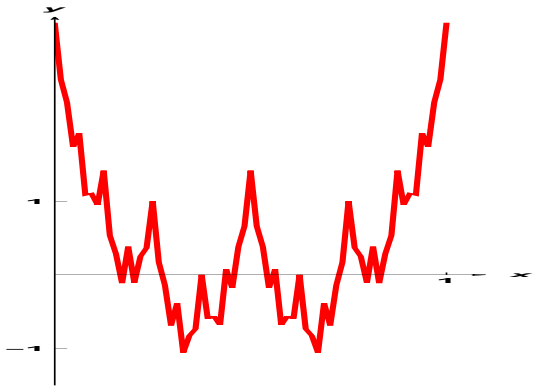

(a) **The prefractal graph $\Gamma_{\mathcal{W}_6}$, in the case when $\lambda = \frac{1}{\sqrt{2}}$ and $N_b = 2$.**

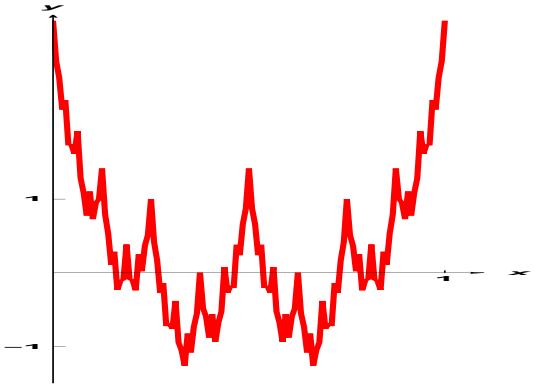

(b) **The prefractal graph $\Gamma_{\mathcal{W}_7}$, in the case when $\lambda = \frac{1}{\sqrt{2}}$ and $N_b = 2$.**

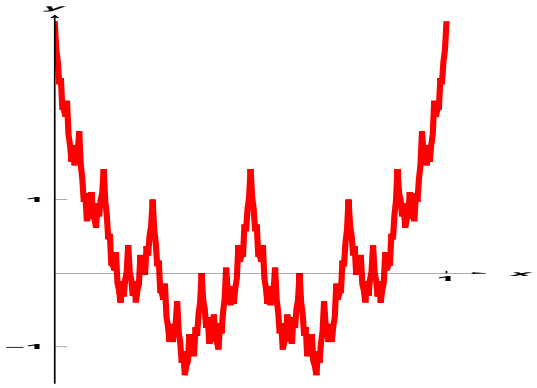

(c) **The prefractal graph $\Gamma_{\mathcal{W}_8}$, in the case when $\lambda = \frac{1}{\sqrt{2}}$ and $N_b = 2$.**

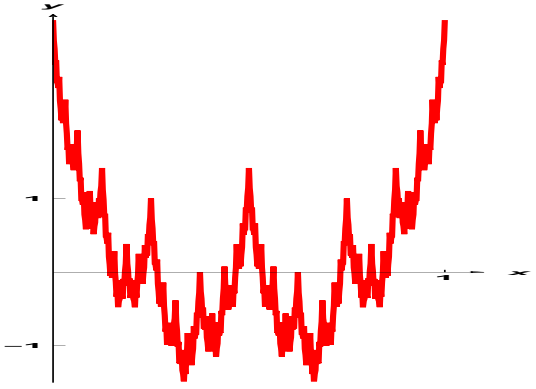

(d) **The prefractal graph $\Gamma_{\mathcal{W}_9}$, in the case when $\lambda = \frac{1}{\sqrt{2}}$ and $N_b = 2$.**

Figure 2: **The prefractal graphs $\Gamma_{\mathcal{W}_6}$, $\Gamma_{\mathcal{W}_7}$, $\Gamma_{\mathcal{W}_8}$, $\Gamma_{\mathcal{W}_9}$ in the case when $\lambda = \frac{1}{\sqrt{2}}$ and $N_b = 2$.**

Property 2.3. *Given $m \in \mathbb{N}$, the number of elements in the finite set V_m is*

$$\#V_m = N_b^m + 1\,.$$

Property 2.4 (**Density of the Set $V^\star = \bigcup_{n\in\mathbb{N}} V_n$ in the Weierstrass Curve [DL24c]**).

The set $V^\star = \bigcup_{n\in\mathbb{N}} V_n$ is dense in the Weierstrass Curve $\Gamma_{\mathcal{W}}$.

Definition 2.4 (**Adjacent Vertices, Edge Relation**).

For any $m \in \mathbb{N}$, the prefractal graph Γ_m is equipped with an edge relation $\underset{m}{\sim}$, as follows: two vertices X and Y of Γ_m; i.e., two points belonging to V_m, are said to be *adjacent* (i.e., neighboring or junction points) if and only if the line segment $[X, Y]$ is an edge of Γ_m ; we then write $X \underset{m}{\sim} Y$. Note that this edge relation depends on m, which means that points adjacent in V_m might not remain adjacent in V_{m+1}.

Definition 2.5 (**Vertices of the Prefractals, Elementary Lengths, Heights and Angles**).

Given a strictly positive integer m, we denote by $\left(\boldsymbol{M_{j,m}}\right)_{\mathbf{0\leqslant j\leqslant (N_b-1)\,N_b^m-1}}$ **the set of vertices** of the prefractal graph Γ_m. For any integer j in $\left\{0, \ldots, (N_b-1)\,N_b^m - 1\right\}$, we denote by $\left(x_{j,m}, \mathcal{W}\left(x_{j,m}\right)\right)$ the coordinates of the vertex $M_{j,m}$:

$$M_{j,m} = \left(x_{j,m}, \mathcal{W}\left(x_{j,m}\right)\right) = \left(\frac{j}{2^m}, \mathcal{W}\left(\frac{j}{2^m}\right)\right).$$

We also introduce, for any integer j in $\left\{0, \ldots, (N_b-1)\,N_b^m - 2\right\}$, the following quantities:

i. the elementary horizontal lengths:

$$L_m = \frac{1}{N_b^m}\,;$$

ii. the elementary lengths:

$$l_{j,m} = d\left(M_{j,m}, M_{j+1,m}\right) = \sqrt{L_m^2 + h_{j,m}^2}\,,$$

where $h_{j,m}$ is defined in *iii.* just below.

iii. the elementary heights:

$$h_{j,m} = \left|\mathcal{W}\left(x_{j+1,m}\right) - \mathcal{W}\left(x_{j,m}\right)\right|\,;$$

note that the absolute value is required, depending on the value taken by j.

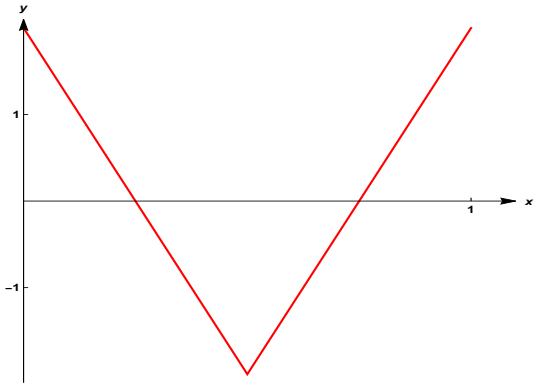

(a) **The prefractal graph $\Gamma_{\mathcal{W}_0}$, in the case when $\lambda = \frac{1}{2}$ and $N_b = 3$.**

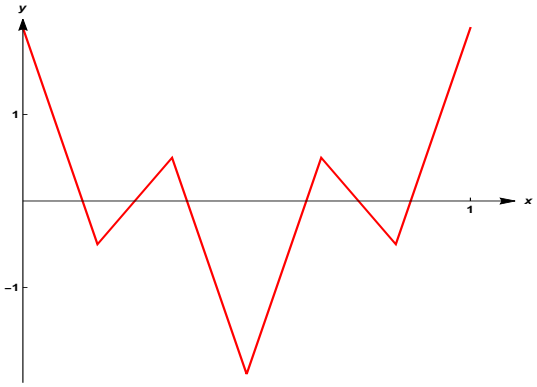

(b) **The prefractal graph $\Gamma_{\mathcal{W}_1}$, in the case when $\lambda = \frac{1}{2}$ and $N_b = 3$.**

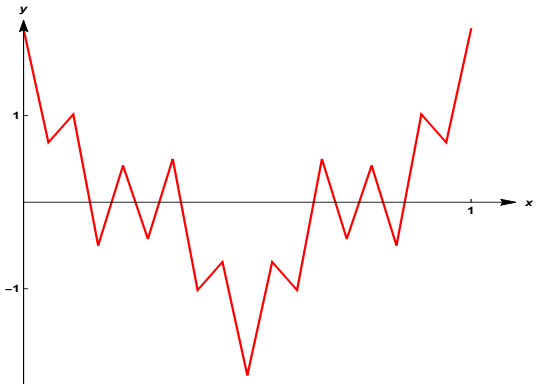

(c) **The prefractal graph $\Gamma_{\mathcal{W}_2}$, in the case when $\lambda = \frac{1}{2}$ and $N_b = 3$.**

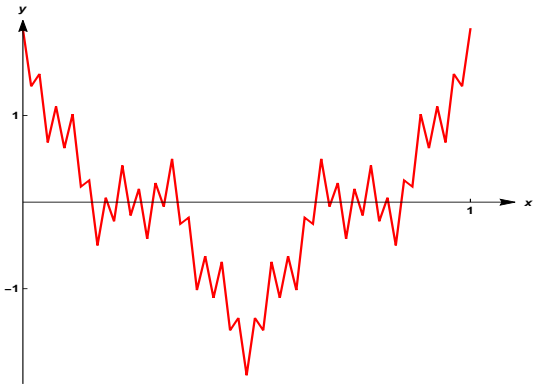

(d) **The prefractal graph $\Gamma_{\mathcal{W}_3}$, in the case when $\lambda = \frac{1}{2}$ and $N_b = 3$.**

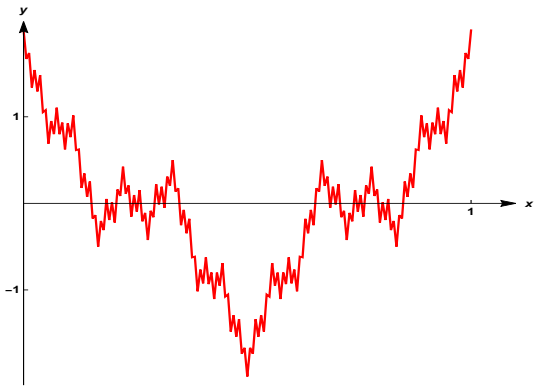

(e) **The prefractal graph $\Gamma_{\mathcal{W}_4}$, in the case when $\lambda = \frac{1}{2}$ and $N_b = 3$.**

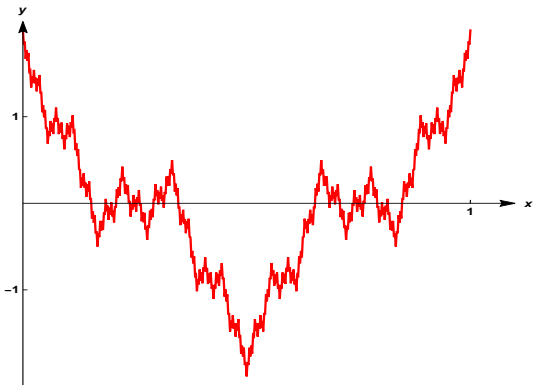

(f) **The prefractal graph $\Gamma_{\mathcal{W}_5}$, in the case when $\lambda = \frac{1}{2}$ and $N_b = 3$.**

Figure 3: **The prefractal graphs $\Gamma_{\mathcal{W}_0}$, $\Gamma_{\mathcal{W}_1}$, $\Gamma_{\mathcal{W}_2}$, $\Gamma_{\mathcal{W}_3}$, $\Gamma_{\mathcal{W}_4}$, $\Gamma_{\mathcal{W}_5}$, in the case when $\lambda = \frac{1}{2}$ and $N_b = 3$.**

iv. the minimal height:

$$h_m^{inf} = \inf_{0 \leqslant j \leqslant (N_b-1)\, N_b^m - 1} h_{j,m}\,, \tag{$\mathcal{R}\,5$}$$

along with the maximal height:

$$h_m = \sup_{0 \leqslant j \leqslant (N_b-1)\, N_b^m - 1} h_{j,m}\,; \tag{$\mathcal{R}\,6$}$$

v. the geometric angles:

$$\theta_{j,m} = \big((Oy), \big(\widehat{M_{j,m} M_{j+1,m}}\big)\big)\,,$$

where (Oy) denotes the vertical axis, which yield **the following value of the geometric angle between consecutive edges**, namely, $\big[M_{j-1,m}\, M_{j,m}, M_{j,m}\, M_{j+1,m}\big]$, with arctan = $\tan^{-1}$:

$$\theta_{j-1,m} + \theta_{j,m} = \arctan \frac{L_m}{h_{j-1,m}} + \arctan \frac{L_m}{h_{j,m}}\,.$$

Note that, of course, $\theta_{j,m} = \arctan \dfrac{L_m}{h_{j,m}}$.

Property 2.5 (**Scaling Properties of the Weierstrass Function, and Consequences**)**.**

Since, for any real number x, $\mathcal{W}(x) = \displaystyle\sum_{n=0}^{\infty} \lambda^n \cos\big(2\,\pi\, N_b^n\, x\big)$, one also has

$$\mathcal{W}(N_b\, x) = \sum_{n=0}^{\infty} \lambda^n \cos\big(2\,\pi\, N_b^{n+1}\, x\big) = \frac{1}{\lambda} \sum_{n=1}^{\infty} \lambda^n \cos\big(2\,\pi\, N_b^n\, x\big) = \frac{1}{\lambda}\, \big(\mathcal{W}(x) - \cos\,(2\,\pi\, x)\big)\,,$$

which yields, for any strictly positive integer m and any j in $\{0, \ldots, \#V_m - 1\}$,

$$\mathcal{W}\big(x_{j,m}\big) = \lambda\, \mathcal{W}\big(x_{j,m-1}\big) + \cos\big(2\,\pi\, x_{j,m}\big)\,.$$

By induction, one then obtains that

$$\mathcal{W}\big(x_{j,m}\big) = \lambda^m\, \mathcal{W}\bigg(\frac{j}{N_b - 1}\bigg) + \sum_{k=0}^{m-1} \lambda^k \cos\big(2\,\pi\, N_b^k\, x_{j,m}\big)\,. \tag{$\mathcal{R}\,7$}$$

By letting

$$t_{j,m} = 2\,\pi\, x_{j,m}\,,$$

we immediately deduce that, for the (equivalent) $2\,\pi$-periodic Weierstrass function introduced in relation ($\mathcal{R}3$), on page 6, we have that

$$\widetilde{\mathcal{W}}\big(t_{j,m}\big) = \lambda^{m-m_0}\, \widetilde{\mathcal{W}}\big(t_{j,m_0}\big) + \sum_{k=0}^{m-m_0-1} \lambda^k \cos\big(N_b^k\, t_{j,m}\big)\,. \tag{$\mathcal{R}\,8$}$$

Proposition 2.6 (**Generalization of [DL25d]**).

For any integer $m_0 \geqslant 1$, any integer $m \geqslant m_0$ and any integer j in $\{0, \ldots, \#V_m - 1\}$,

$$C_{inf}\,(m_0, N_b)\;\lambda^{m-m_0} \leqslant \left|\mathcal{W}\left(x_{j+1,m}\right) - \mathcal{W}\left(x_{j,m}\right)\right| \leqslant C_{sup}\,(m_0, N_b)\;\lambda^{m-m_0} \quad , \quad m \in \mathbb{N},\, 0 \leqslant j \leqslant 2^{m-1}, \tag{$\mathcal{R}$9}$$

where

$$C_{inf}\,(m_0, N_b) = \min_{0 \leqslant j \leqslant N_b^{m_0}-1,\, \mathcal{W}\left(\frac{j+1}{N_b^{m_0}}\right) \neq \mathcal{W}\left(\frac{j}{N_b^{m_0}}\right)} \left|\mathcal{W}\left(\frac{j+1}{N_b^{m_0}}\right) - \mathcal{W}\left(\frac{j}{N_b^{m_0}}\right)\right| .$$

and

$$C_{sup}\,(m_0, N_b) = \left(\max_{0 \leqslant j \leqslant N_b^{m_0}-1} \left|\mathcal{W}\left(\frac{j+1}{N_b^{m_0}}\right) - \mathcal{W}\left(\frac{j}{N_b^{m_0}}\right)\right| + \frac{2\,\pi}{N_b^{m_0}\,(\lambda\, N_b - 1)}\right) .$$

Similarly, for the (equivalent) $2\,\pi$-periodic Weierstrass function introduced in relation ($\mathcal{R}$3), on page 6, we have that, for any integer $m \geqslant m_0$, and any integer j in $\{0, \ldots, \#V_m - 1\}$,

$$\widetilde{C}_{inf}\,(m_0, N_b)\;\lambda^{m-m_0} \leqslant \left|\widetilde{\mathcal{W}}\left(t_{j+1,m}\right) - \widetilde{\mathcal{W}}\left(t_{j,m}\right)\right| \leqslant \widetilde{C}_{sup}\,(m_0, N_b)\;\lambda^{m-m_0} \quad , \quad m \in \mathbb{N},\, 0 \leqslant j \leqslant N_b^{m-1}, \tag{$\mathcal{R}$10}$$

where

$$\widetilde{C}_{inf}\,(m_0, N_b) = \min_{0 \leqslant j \leqslant N_b^{m_0}-1,\, \mathcal{W}\left(\frac{j+1}{2}\right) \neq \mathcal{W}\left(\frac{j}{2}\right)} \left|\mathcal{W}\left(\frac{j+1}{N_b^{m_0}}\right) - \mathcal{W}\left(\frac{j}{N_b^{m_0}}\right)\right| .$$

and

$$\widetilde{C}_{sup}\,(m_0, N_b) = \left(\max_{0 \leqslant j \leqslant N_b^{m_0}-1} \left|\mathcal{W}\left(\frac{j+1}{N_b^{m_0}}\right) - \mathcal{W}\left(\frac{j}{N_b^{m_0}}\right)\right| + \frac{1}{N_b^{m_0}\,(\lambda\, N_b - 1)}\right) .$$

Proof. Thanks to relation ($\mathcal{R}$7), on page 13, given $m_0 \geqslant 1$, we have, for any integer $m \geqslant m_0$ and any j in $\left\{0, \ldots, N_b^m\right\}$, the following estimates:

$$\begin{aligned} \left|\mathcal{W}\left(x_{j+1,m}\right) - \mathcal{W}\left(x_{j,m}\right)\right| \;&\leqslant\; \lambda\, \left|\mathcal{W}\left(x_{j+1,m-1}\right) - \mathcal{W}\left(x_{j,m-1}\right)\right| \\ &\quad + \left|\cos\left(2\,\pi\, x_{j+1,m}\right) - \cos\left(2\,\pi\, x_{j,m}\right)\right| . \end{aligned}$$

Since

$$\begin{aligned} \left|\cos\left(2\,\pi\, x_{j+1,m}\right) - \cos\left(2\,\pi\, x_{j,m}\right)\right| \;&=\; 2\, \left|\sin\left(\pi\, \left(x_{j+1,m-1} + x_{j+1,m-1}\right)\right) \sin\left(\pi\, \left(x_{j+1,m} - x_{j+1,m-1}\right)\right)\right| \\ &=\; 2\, \left|\sin\left(\pi\, \left(x_{j+1,m-1} + x_{j+1,m}\right)\right) \sin\left(\frac{\pi}{N_b^m}\right)\right| \\ &\leqslant\; \frac{2\,\pi}{N_b^m} \end{aligned}$$

we then obtain that

$$\left|\mathcal{W}\left(x_{j+1,m}\right)-\mathcal{W}\left(x_{j,m}\right)\right| \;\leqslant\; \lambda\,\left|\mathcal{W}\left(x_{j+1,m}\right)-\mathcal{W}\left(x_{j,m}\right)\right|+\frac{2\,\pi}{N_b^m}\,,$$

which yields, by induction,

$$\begin{aligned}\left|\mathcal{W}\left(x_{j+1,m}\right)-\mathcal{W}\left(x_{j,m}\right)\right| &\leqslant \lambda^{m-m_0}\left|\mathcal{W}\left(\frac{j+1}{N_b^{m_0}}\right)-\mathcal{W}\left(\frac{j}{N_b^{m_0}}\right)\right|+\sum_{k=0}^{m-m_0-1}\lambda^k\,\frac{2\,\pi\,N_b^k}{N_b^m}\\ &\leqslant \lambda^{m-m_0}\left|\mathcal{W}\left(\frac{j+1}{2^{m_0}}\right)-\mathcal{W}\left(\frac{j}{N_b^{m_0}}\right)\right|+\frac{2\,\pi\,N_b^{m-m_0}\,\lambda^{m-m_0}}{N_b^m\,(\lambda\,N_b-1)}\\ &= \lambda^{m-m_0}\left(\left|\mathcal{W}\left(x_{j+1,m_0}\right)-\mathcal{W}\left(x_{j,m_0}\right)\right|+\frac{2\,\pi}{N_b^{m_0}\,(\lambda\,N_b-1)}\right),\end{aligned}$$

as claimed.

In a similar manner, we also obtain that, for any integer $m \geqslant 2$ and any j in $\left\{0,\ldots,N_b^m\right\}$,

$$\begin{aligned}\left|\widetilde{\mathcal{W}}\left(t_{j+1,m}\right)-\widetilde{\mathcal{W}}\left(t_{j,m}\right)\right| &\leqslant \lambda\,\left|\widetilde{\mathcal{W}}\left(t_{j+1,m-1}\right)-\widetilde{\mathcal{W}}\left(t_{j,m-1}\right)\right|\\ &\quad+\left|\cos\left(t_{j+1,m-1}\right)-\cos\left(t_{j,m-1}\right)\right|\,,\end{aligned}$$

which yields, by induction,

$$\left|\widetilde{\mathcal{W}}\left(t_{j+1,m}\right)-\widetilde{\mathcal{W}}\left(t_{j,m}\right)\right| \;\leqslant\; \lambda^{m-m_0}\left(\left|\widetilde{\mathcal{W}}\left(t_{j+1,m_0}\right)-\widetilde{\mathcal{W}}\left(t_{j,m_0}\right)\right|+\frac{1}{N_b^{m_0}\,(\lambda\,N_b-1)}\right),$$

as desired.

□

Corollary 2.7 (**(of Proposition 2.6) Local Extrema [DL25d]**).

i. The set of local maxima of the Weierstrass function on the interval $[0,1]$ *is given by*

$$\left\{\left(\frac{(N_b-1)\,k}{N_b^m},\mathcal{W}\left(\frac{(N_b-1)\,k}{N_b^m}\right)\right)\,:\,0\leqslant k\leqslant N_b^m-1,\,m\,\in\,\mathbb{N}\right\}.$$

ii. For odd values of N_b*, the set of local minima of the Weierstrass function on the interval* $[0,1]$ *is given by*

$$\left\{\left(\frac{(N_b-1)\,k+\frac{N_b-1}{2}}{(N_b-1)\,N_b^m},\mathcal{W}\left(\frac{(N_b-1)\,k+\frac{N_b-1}{2}}{(N_b-1)\,N_b^m}\right)\right)\,:\,0\leqslant k\leqslant N_b^m-1,\,m\,\in\,\mathbb{N}\right\}.$$

Remark 2.1. Note that, if we deal with the specific case where $N_b = 2$, and in contrast to our previous works concerning the case $N_b \geqslant 3$, the right-hand side of the scaling relation ($\mathcal{R}7$) above lies between $\mathcal{W}\left(x_{j,m}\right)$ and $\mathcal{W}\left(x_{j,m_0}\right)$. Consequently, the exponent of λ is $m - m_0$, and the sum that follows stops at $m - m_0 - 1$.

The reason is that, if we denote by m_0 the value for the integer beginning the induction, we require distinct $\mathcal{W}\left(x_{j,m_0}\right)$, $j \in \{1, 2\}$. When $N_b = 2$, however, the values $\mathcal{W}\left(x_{0,0}\right)$ and $\mathcal{W}\left(x_{0,0}\right)$ are equal. Hence, the value $m_0 = 1$ works.

In addition, our more general results in Proposition 2.6 above will enable us to obtain sharper estimates for the the Lip $\left(\frac{1}{2}\right)$ norm of the Weierstrass function, as we now explain.

Theorem 2.8 (Lip (δ) **Norm of the Weierstrass Function**)**.**

Given $\delta \in \left]0, \frac{1}{2}\right]$, *for the value* $\lambda = \frac{1}{\sqrt{N_b}}$, *the* Lip (δ) *norm* $\|\mathcal{W}\|_\delta = \sup_{x \in \mathbb{R}} \sup_{h>0} \frac{|\mathcal{W}(x+h) - \mathcal{W}(x)|}{h^\delta}$ *of the Weierstrass function satisfies*

$$(N_b - 1)^\delta \, \lambda^{-m_0} \, C_{inf}\left(m_0, N_b\right) \leqslant \|\mathcal{W}\|_\delta \leqslant (N_b - 1)^\delta \, \lambda^{-m_0} \, C_{sup}\left(m_0, N_b\right) , \qquad (\mathcal{R}\,11)$$

with $m_0 \geqslant 1$, *and where the strictly positive constants* $C_{inf}\left(m_0, N_b\right)$ *and* $C_{sup}\left(m_0, N_b\right)$ *are given in the first part of Proposition 2.6, on page 14.*

By choosing an optimal induction level m_0, *we then obtain sharp estimates for the* Lip (δ) *norm of the Weierstrass function.*

Similarly, the Lip (δ) *norm* $\|\widetilde{\mathcal{W}}\|_{\frac{1}{2}} = \sup_{t \in \mathbb{R}} \sup_{h>0} \frac{\left|\widetilde{\mathcal{W}}(t+h) - \widetilde{\mathcal{W}}(t)\right|}{h^\delta}$ *of the (equivalent)* $2\,\pi$*-periodic Weierstrass function* $\widetilde{\mathcal{W}}$ *(given in relation (*$\mathcal{R}3$*)) satisfies,*

$$(N_b - 1)^\delta \, \lambda^{-m_0} \, \widetilde{C}_{inf}\left(m_0, N_b\right) \leqslant \|\widetilde{\mathcal{W}}\|_{\frac{1}{2}} \leqslant (N_b - 1)^\delta \, \lambda^{-m_0} \, \widetilde{C}_{sup}\left(m_0, N_b\right) , \qquad (\mathcal{R}\,12)$$

where $m_0 \geqslant 1$ *is optimal, and where the strictly positive constants* $\widetilde{C}_{inf}\left(m_0, N_b\right)$ *and* $\widetilde{C}_{sup}\left(m_0, N_b\right)$ *are given in the latter part of Proposition 2.6, on page 14.*

Corollary 2.9 (Lip $\left(\frac{1}{2}\right)$ **Norm of the Weierstrass Function, in the Case** $N_b = 2$)**.**

When $N_b = 2$, *for the value* $\lambda = \frac{1}{\sqrt{2}}$, *the* Lip $\left(\frac{1}{2}\right)$ *norm* $\|\mathcal{W}\|_{\frac{1}{2}} = \sup_{x \in \mathbb{R}} \sup_{h>0} \frac{|\mathcal{W}(x+h) - \mathcal{W}(x)|}{\sqrt{h}}$ *of the Weierstrass function, given, for all* $x \in \mathbb{R}$, *by*

$$\mathcal{W}(x) = \sum_{n=0}^{\infty} 2^{-\frac{n}{2}} \, \cos\left(2\,\pi \times 2^n \, x\right) ,$$

satisfies

$$\lambda^{-m_0} \, C_{inf}\left(m_0, 2\right) \leqslant \|\mathcal{W}\|_{\frac{1}{2}} \leqslant \lambda^{-m_0} \, C_{sup}\left(m_0, 2\right) , \qquad (\mathcal{R}\,13)$$

with $m_0 \geqslant 1$, and where the strictly positive constant $C_{inf}(m_0, 2)$ and $C_{sup}(m_0, 2)$ are given in the first part of Proposition 2.6, on page 14, with $N_b = 2$.

Similarly, the $\mathrm{Lip}\left(\frac{1}{2}\right)$ *norm* $\|\widetilde{\mathcal{W}}\|_{\frac{1}{2}} = \sup_{x \in \mathbb{R}} \sup_{h>0} \dfrac{|\mathcal{W}(x+h) - \mathcal{W}(x)|}{\sqrt{h}}$ *of the (equivalent)* 2π*-periodic Weierstrass function* $\widetilde{\mathcal{W}}$ *given, for all* $t \in \mathbb{R}$*, by*

$$\widetilde{\mathcal{W}}(t) = \sum_{n=0}^{\infty} 2^{-\frac{n}{2}} \cos\left(2^n t\right) ,$$

satisfies,

$$\lambda^{-m_0}\, \widetilde{C}_{inf}(m_0, 2) \leqslant \|\widetilde{\mathcal{W}}\|_{\frac{1}{2}} \leqslant \lambda^{-m_0}\, \widetilde{C}_{sup}(m_0, 2) , \qquad (\mathcal{R}\,14)$$

with $m_0 \geqslant 1$, and where the strictly positive constants $\widetilde{C}_{inf}(m_0, 2)$ and $\widetilde{C}_{sup}(m_0, 2)$ are given in the latter part of Proposition 2.6, on page 14, with $N_b = 2$.

Remark 2.2. The estimate in Corollary 2.9 above enables us to obtain optimal numerical bounds for the values of the $\mathrm{Lip}\left(\frac{1}{2}\right)$ norms $\|\mathcal{W}\|_{\frac{1}{2}}$ and $\|\widetilde{\mathcal{W}}\|_{\frac{1}{2}}$. One simply has to choose the optimal value of the integer m_0, which is obtained for the choice $m_0 = 3$, and yields

$$1.53637 \leqslant \|\widetilde{\mathcal{W}}\|_{\frac{1}{2}} \leqslant 5.94595 , \qquad (\mathcal{R}\,15)$$

i.e., a much better estimate than the values 0.245 and 11.66 given in [LR17]. We note that our bounds correspond to the numerical experimental data displayed in [LR17], which are between 2 and 5.

Proof. (**of Theorem 2.8**])

We simply use the estimates obtained in Proposition 2.6, on page 14.

First, we note that, given an integer $m \in \mathbb{N}^\star$, for all $x \in \mathbb{R}$ and any $h > 0$, we have that

$$|\mathcal{W}(x+h) - \mathcal{W}(x)| \;=\; \left| \mathcal{W}\left(\frac{N_b^m\, h\, x}{N_b^m\, h} + \frac{N_b^m\, h}{N_b\, (N_b - 1)\, N_b^m} \right) - \mathcal{W}\left(\frac{N_b^m\, h}{N_b^m} \right) \right|$$

By letting

$$x' = \frac{N_b^m\, h\, x}{h} \quad \text{and} \quad h' = N_b^m\, h ,$$

we can write

$$|\mathcal{W}(x+h) - \mathcal{W}(x)| \;=\; \left| \mathcal{W}\left(x' + \frac{h'}{(N_b - 1)\, N_b^m} \right) - \mathcal{W}\left(\frac{h'}{(N_b - 1)\, N_b^m} \right) \right| ,$$

so that, by 1-periodicity,

$$
\begin{aligned}
\|\mathcal{W}\|_{\delta} &= \sup_{x\in[0,1]}\ \sup_{h>0} \frac{|\mathcal{W}(x+h)-\mathcal{W}(x)|}{h} \\
&= \sup_{0\leqslant x'+\frac{h'}{(N_b-1)\,N_b^m}\leqslant 1} \frac{\left|\mathcal{W}\left(x'+\dfrac{h'}{(N_b-1)\,N_b^m}\right)-\mathcal{W}\left(\dfrac{h'}{(N_b-1)\,N_b^m}\right)\right|}{\left(\dfrac{h'}{(N_b-1)\,N_b^m}\right)^{\delta}} \\
&= \sup_{0\leqslant x'+\frac{h'}{(N_b-1)\,N_b^m}\leqslant 1} \frac{\left|\mathcal{W}\left(x'+\dfrac{h'}{(N_b-1)\,N_b^m}\right)-\mathcal{W}\left(\dfrac{h'}{(N_b-1)\,N_b^m}\right)\right|}{\left(\dfrac{h'}{(N_b-1)\,N_b^m}\right)^{\delta}}.
\end{aligned}
$$

By relying on the fact that the set

$$
\left(x_{j,m}\right)_{0\leqslant j\leqslant \#V_m-1,\, m\geqslant 1} = \left(\frac{j}{(N_b-1)\,N_b^m}\right)_{0\leqslant j\leqslant \#V_m-1,\, m\geqslant 1}
$$

is dense in $[0,1]$, we thus deduce that

$$
\begin{aligned}
\|\mathcal{W}\|_{\delta} &= \sup_{m\geqslant 1} \frac{\left|\mathcal{W}\left(x_{j,m}+\dfrac{1}{(N_b-1)\,N_b^m}\right)-\mathcal{W}\left(x_{j,m}\right)\right|}{\left(\dfrac{1}{(N_b-1)\,N_b^m}\right)^{\delta}} \\
&= \sup_{m\geqslant 1} (N_b-1)^{\delta}\ \frac{\left|\mathcal{W}\left(x_{j,m}+\dfrac{1}{(N_b-1)\,N_b^m}\right)-\mathcal{W}\left(x_{j,m}\right)\right|}{\left(\dfrac{1'}{(N_b-1)\,N_b^m}\right)^{\delta}}.
\end{aligned}
$$

Now, for any integer $m_0 \geqslant 1$, any integer $m \geqslant m_0$ and any integer j in $\{0,\ldots,\#V_m-1\}$, we have that, for $0 \leqslant j \leqslant \#V_m - 1$,

$$
C_{inf}\,(m_0,N_b)\ \lambda^{m-m_0} \leqslant \left|\mathcal{W}\left(x_{j,m}+\frac{1}{(N_b-1)\,N_b^m}\right)-\mathcal{W}\left(\frac{1}{(N_b-1)\,N_b^m}\right)\right| \leqslant C_{sup}\,(m_0,N_b)\ \lambda^{m-m_0}\ , \tag{$\mathcal{R}$ 16}
$$

where

$$
x_{j+1,m} = x_{j,m} + \frac{1}{(N_b-1)\,N_b^m}\,.
$$

By choosing the parameter λ such that

$$
\lambda = \frac{1}{{N_b}^{\delta}}\,,
$$

we then deduce that

$$
\lambda^{-m_0}\,C_{inf}\,(m_0,N_b) \leqslant \sup_{m\geqslant 1} \frac{\left|\mathcal{W}\left(x_{j,m}+\dfrac{1}{(N_b-1)\,N_b^m}\right)-\mathcal{W}\left(\dfrac{1}{(N_b-1)\,N_b^m}\right)\right|}{\left(\dfrac{1}{N_b^m}\right)^{\delta}} \leqslant \lambda^{-m_0}\,C_{sup}\,(m_0,N_b)\ , \tag{$\mathcal{R}$ 17}
$$

which immediately ensures that

$$(N_b-1)^{\delta}\ \lambda^{-m_0}\,C_{inf}\,(m_0,N_b)\leqslant \sup_{m\geqslant 1}\frac{\left|\mathcal{W}\left(x_{j,m}+\frac{1}{(N_b-1)\,N_b^m}\right)-\mathcal{W}\left(\frac{1}{(N_b-1)\,N_b^m}\right)\right|}{\left(\frac{1}{)(N_b-1)\,N_b^m}\right)^{\delta}}\leqslant (N_b-1)^{\delta}\ \lambda^{-m_0}\,C_{sup}\,(m_0,N_b)\ , \tag{$\mathcal{R}$ 18}$$

and, consequently,

$$(N_b-1)^{\delta}\ \lambda^{-m_0}\,C_{inf}\,(m_0,N_b)\leqslant \|\mathcal{W}\|_{\delta}=\sup_{x\,\in\,[0,1]}\sup_{h>0}\frac{|\mathcal{W}(x+h)-\mathcal{W}(x)|}{h^{\delta}}\leqslant (N_b-1)^{\delta}\ \lambda^{-m_0}\,C_{sup}\,(m_0,N_b)\ . \tag{$\mathcal{R}$ 19}$$

Similarly, we obtain that

$$(N_b-1)^{\delta}\ \lambda^{-m_0}\,\widetilde{C}_{inf}\,(m_0,N_b)\leqslant \|\widetilde{\mathcal{W}}\|_{\delta}=\sup_{x\,\in\,[0,2\,\pi]}\sup_{h>0}\frac{\left|\widetilde{\mathcal{W}}(x+h)-\widetilde{\mathcal{W}}(x)\right|}{h^{\delta}}\leqslant (N_b-1)^{\delta}\ \lambda^{-m_0}\,\widetilde{C}_{sup}\,(m_0,N_b)\,,. \tag{$\mathcal{R}$ 20}$$

□

The results above (in Theorem 2.8, on page 16, are all the more important, as they enable us to obtain more precise bounds for the values of the real parameter c such that the Weierstrass drift, of the form

$$t\mapsto \lambda(t)=c\,\widetilde{\mathcal{W}}(t)\,,$$

generates (in the sense of the traces of SLE_{κ} – *the hull*) consist of simple or multiple curves.

In [LR17], due to their bounds of the Lip $\left(\frac{1}{2}\right)$ norm $\|\widetilde{\mathcal{W}}\|_{\frac{1}{2}}$, in the case when $N_b=2$ and $\lambda=\dfrac{1}{\sqrt{2}}$, given by

$$0.245\leqslant \|\widetilde{\mathcal{W}}\|_{\frac{1}{2}}\leqslant 12$$

and in order to satisfy the condition (given in [Lin05]),

$$\|c\,\widetilde{\mathcal{W}}\|_{\frac{1}{2}}<4\,,$$

the authors obtain the following conditions:

i. for a hull consisting of simple curves: $c<\dfrac{1}{3}$;

ii. for a hull consisting of multiple curves: $c\geqslant 20$.

Recall that

$$\|c\,\widetilde{\mathcal{W}}\|_{\frac{1}{2}}=c\,\|\widetilde{\mathcal{W}}\|_{\frac{1}{2}}\,.$$

Therefore, with our results in Theorem 2.8, on page 16 (see also Table 1 for the corresponding numerical values), and in order to satisfy the condition (given in [Lin05]),

$$\|c\,\widetilde{\mathcal{W}}\|_{\frac{1}{2}}<4\,,$$

we therefore obtain the corresponding critical value, given by

$$c = \frac{4}{||\widetilde{\mathcal{W}}||_{\frac{1}{2}}},$$

along with the following improved, sharper condition:

i. for a hull consisting of simple curves: $c < 0.672$;

ii. for a hull consisting of multiple curves: $c > 0.672$.

Since the lower and upper bounds for the relevant Lip $\left(\frac{1}{2}\right)$ norm $||\widetilde{\mathcal{W}}||_{\frac{1}{2}}$ coincide, they induce the same value of the critical scaling parameter, which is uniquely determined as

$$c = 0.672\ldots,$$

thereby providing the exact threshold between simple and nonsimple hulls.

Note that our result is also better than the results that can be found, for only $N_b = 2$, in [Lin05]. They are also better than the results that can be found in the PhD Dissertation of David N. Horton in [Hor18], Chapter 3, in the case when $N_b = 3$ and $\lambda = \frac{1}{\sqrt{3}}$, where, by placing himself along the lines of what is done in [Lin05], she obtains, after a very heavy computation, an approximate, inexplicit upper bound (involving a limit). No lower bound is provided.

In our case, the estimate in Theorem 2.8 above enables us to obtain optimal numerical bounds for the values of the Lip $\left(\frac{1}{2}\right)$ norms $||\mathcal{W}||_{\frac{1}{2}}$ and norms $||\widetilde{\mathcal{W}}||_{\frac{1}{2}}$. Again, one simply has to choose the optimal value of the integer m_0, which are respectively obtained for the choice $m_0 = 4$ for the lower bound and $m_0 = 3$ for the upper bound, and yields

$$0.4510888 \leqslant ||\widetilde{\mathcal{W}}||_{\frac{1}{2}} \tag{$\mathcal{R}$ 21}$$

$$||\widetilde{\mathcal{W}}||_{\frac{1}{2}} \leqslant 5.94595\,, \tag{$\mathcal{R}$ 22}$$

i.e., explicit estimates.

The comparison between our results and the values obtained in [LR17] is summarized in Table 1. The comparison of the thresholds for phase transition is given is Table 2.

We note that we explicitly obtain the value of the phase transition threshold, contrary to the large, rough estimate of $c > 20$ given in [LR17], which is not obtained by relying on precise estimates for the Lip $\left(\frac{1}{2}\right)$ norms $||\mathcal{W}||_{\frac{1}{2}}$ and norms $||\widetilde{\mathcal{W}}||_{\frac{1}{2}}$. This rough, unprecise estimate is obtained by means of their value 0.2 for the lower bound. Note that their upper bound of 12 would have provided a wrong threshold of $\frac{1}{3}$, as it can be noticed in the figures which can be observed in Figure 2, on page 153, in [LR17], with multiple curves already for $c \geqslant 1.2$.

Another important comment concerns the computation of the plots displayed in Figure 2, on page 153, in [LR17]. No details are given with respect to the numerical implementation. We guess that the author rely on a truncation of the trigonometric series which defines the Weierstrass function, which implicitly adds a distortion in the resulting traces.

This naturally raises the question of the connections between the regularity properties of the drift, and the geometry of the resulting trace, which will be studied in Section 3.

Reference	Lower Bound	Upper Bound	Comment
[LR17]	0.245	11.66	Wide bounds, obtained by truncation
Present work ($m_0 = 3$)	1.536	5.946	Net improvement: lower bound is close to digital data
Present work($m_0 = 4$)	0.451	7.237	Better explicit upper bound

Table 1: **Comparaison of the** $\mathrm{Lip}\left(\frac{1}{2}\right)$ **bounds, in the case of the Weierstrass drift.**

Reference	Phase transition threshold
[LR17]	$c < \frac{1}{3}$, $c > 20$
Present work	$c = 0.672$

Table 2: **Comparaison of the phase transition threshold, in the case of the Weierstrass drift.**

3 Weierstrass-Driven *SLE* Hulls

3.1 Weierstrass Prefractal Functions – Weierstrass Truncated Functions

Given $T > 0$, we are interested in the solution $g : [0,T] \times \mathbb{H} \to \mathbb{C}$ of the chordal backward Loewner (partial) differential equation (in short, Loewner equation),

$$\forall\, (t,z) \in [0,T] \times \mathbb{H} : \quad \frac{\partial g}{\partial t} = -\frac{2}{g(t,z) - c\,\mathcal{W}(t)} \qquad , \qquad (\mathcal{L}_{\mathcal{W}})$$

where $\mathbb{H} = \{z = x + i\,y\,, \mathcal{I}m(z) = y > 0\}$ denotes the upper half-plane, $\mathcal{W}$ the Weierstrass function (see Definition 2.1), c is a strictly positive real number, with the initial condition $g(t_0, z) = z$. Note that, as it can be found in the literature, the factor 2 can easily be changed into 1 by means of a renormalization.

Given $t \in [0,T]$, we define *the hull* K_t as the two-dimensional domain such that

$$K_t = \left\{ z \in \overline{\mathbb{H}}\,,\, g(s,z) = \mathcal{W}(s) \quad \text{for some } s \leqslant t \right\}. \qquad (\mathcal{R}\,23)$$

As was previously mentioned, in the results given in [LR17], no details are given with respect to the numerical implementation, which suggests the use of a truncated Weierstrass sum.

Definition 3.1 (**Weierstrass Truncated Function**)**.**

Given $N \geqslant 1$, we consider the *Weierstrass truncated function* $\mathcal{W}_N$, defined, for any real number x, by

$$\mathcal{W}_N^{trunc}(x) = \sum_{n=0}^{N} \lambda^n \cos\left(2\,\pi\,N_b^n\,x\right)\,. \tag{$\mathcal{R}$ 24}$$

For the sake of comparison with the results in [LR17], we also introduce *the (equivalent)* $2\,\pi$*-periodic Weierstrass function*, defined, for any real number t, by

$$\widetilde{\mathcal{W}}_N^{trunc}(t) = \mathcal{W}_N^{trunc}\left(\frac{t}{2\,\pi}\right) = \sum_{n=0}^{N} \lambda^n \cos\left(N_b^n\,t\right)\,. \tag{$\mathcal{R}$ 25}$$

In light of our previous works([DL25d], [DL24c], [DL24a], [DL25a], [DL24b], [DL25b], [DL25c]),the Weierstrass Curve can be approximated by means of a convergent sequence of finite polygonal graphs – the so-called *prefractals* – with, of course, associated Weierstrass prefractal functions (see Definition 3.2 below) which are piecewise linear and, very interestingly, δ-Hölder, with $0 < \delta \leqslant \dfrac{1}{2}$ (thanks to Proposition 2.6). A very important characteristic of those prefractal graphs is that their associated sets of vertices are, also, points which belong to the Weierstrass Curve. Moreover, the exact coordinates of those vertices are known (see Property 2. 11 of [DL25d]). In addition, and very interestingly, we have highlighted a phenomenon of *phase transition* associated with the sequence of prefractal approximations, which, for all $m \in \mathbb{N}^\star$ sufficiently large (i.e., for all $m \geqslant m_0$, with $m_0 \in \mathbb{N}^\star$ optimal), are not only fractal (i.e., have nonreal Complex Dimensions) in the sense of ([LvF00], [LvF13], [LRŽ17], [Lap19]), but are also fractal in increasingly many dimensions $d_k = D_{\mathcal{W}} - k\,\left(2 - D_{\mathcal{W}}\right)$, for $0 \leqslant k \leqslant m$ (i.e., have nonreal Complex Dimensions with real part d_k, in the sense of [LRŽ17], [Lap19]); note that $d_k \to -\infty$ as $k \to \infty$. As we explain in [DL25d], this is both natural and important from a physical point of view since, clearly, ideal mathematical fractals do not exist in nature, but are increasingly well approximated by fractal-like objects (here, their natural prefractal approximations).

Definition 3.2 (**Weierstrass Prefractal Function**)**.**

Given $N \geqslant 1$, we consider the *Weierstrass prefractal function* $\mathcal{W}_N$, defined, for any real number x, by

$$\begin{aligned}\mathcal{W}_N(x) \;=\; \sum_{j=0}^{(N_b-1)\,N_b^N-1} \Bigg(& (N_b-1)\,N_b^N \left(\mathcal{W}\left(\frac{j+1}{(N_b-1)\,N_b^N}\right) - \mathcal{W}\left(\frac{j}{(N_b-1)\,N_b^N}\right)\right) x + \mathcal{W}\left(\frac{j}{(N_b-1)\,N_b^N}\right) \\ & -j\left(\mathcal{W}\left(\frac{j+1}{(N_b-1)\,N_b^N}\right) - \mathcal{W}\left(\frac{j}{(N_b-1)\,N_b^N}\right)\right) \mathbb{1}_{\left[\frac{j}{(N_b-1)\,N_b^N}, \frac{j+1}{(N_b-1)\,N_b^N}\right]}\Bigg)\,.\end{aligned} \tag{$\mathcal{R}$ 26}$$

Again, for the sake of comparison with the results in [LR17], we also introduce *the (equivalent)* $2\,\pi$*-periodic Weierstrass function*, defined, for any real number t, by

$$\widetilde{\mathcal{W}}_N(t) = \mathcal{W}_N\left(\frac{t}{2\,\pi}\right)\,. \tag{$\mathcal{R}$ 27}$$

For the aforementioned reasons, we are therefore able to conduct a comparative study, in the case of Weierstrass-prefractal driven hulls – when the drift is a (piecewise linear) Weierstrass-prefractal

function – and in the case of Weierstrass-truncated driven hulls – when the drift is a sharp truncation of the Weierstrass function (see Definition 3.1 above). For this purpose, we have adapted the method given by Huy Tran in [Tra15]. We worked with a partition of the unit time interval, of the following form,

$$[0,1] = \bigcup_{0 \leqslant k \leqslant N_t - 1} \left[\frac{k}{N_t}, \frac{k+1}{N_t} \right],$$

with $N_t \in \mathbb{N}^\star$ large enough (i.e., $N_t \geqslant N_0$, for some $N_0 \in \mathbb{N}^\star$ optimal). The method consists in a variant of the Marshall and Rohde algorithm given in [**?**], and is based on the already mentioned fact according to which in the case of a driving function of square-root affine type, the exact solutions for the Loewner equation can be obtained. We thus simply have to use a sufficiently fine partition of the unit interval, so that, on each subtime interval, we can approximate the (Weierstrass prefractal or truncated) drift by a square-root affine type function. Note that both our Weierstrass prefractal or truncated functions, in the case when $\lambda = \dfrac{1}{\sqrt{2}}$, $N_b = 2$, are Hölder continuous with exponent $\dfrac{1}{2}$, which ensures the convergence of the algorithm; see [**?**].

The corresponding plots, obtained with *Mathematica* (Wolfram) – both of the graph of the driving function and of the associated hull, when $\lambda = \dfrac{1}{\sqrt{2}}$, $N_b = 2$, $c = 1.8$ – are given in Figures 6, 5, 10, 11.

As for the phase transition (simple vs nonsimple hulls), which occurs for $c = 0.65$, in the case of a Weierstrass-prefractal drift, it can be observed in Figures 7 and 9.

By convention, and for the sake of readability, our traces/hulls are represented after reflection with respect to the imaginary axis. This purely geometric transformation does not change the underlying dynamics of the Loewner equation.

We note that:

i. There is a correlation between the *roughness* of the drift, and the resulting hull.

ii. In the case of the Weierstrass prefractal drift, for sufficiently large values of the *polygonal depth* N, the resulting hull is a space-filling curve, a phenomenon which is less noticeable in the case of the Weierstrass-truncated drift, and in the plots provided in Figure 2, on page 153, in [LR17].

iii. As for the phase transition, the threshold $c = 0.672$ can be clearly observed in the case of the Weierstrass prefractal drift, which is not the case when the drift is a Weierstrass truncated function, as in part *a*. of the plots displayed in Figure 12, or as in [Lin05], Figure 2, on page 153. This suggests that the Weierstrass prefractal function is a better suited drift than the Weierstrass truncated function for capturing the fine structure of hulls. In particular, the Weierstrass truncated function is a smooth function, contrary to the Weierstrass prefractal function.

3.2 Multifractal formalism

We hereafter proceed as is done by Nikolai G. Makarov in [Mak98]. Given an atom-free probability measure μ with compact support $\mathcal{F} \subset \mathbb{R}^2$, the aim is to obtain the so-called *packing spectrum* – or, equivalently, the *entropy function* – defined, for all $t \in \mathbb{R}$, by

$$\pi(t) = \sup \left\{ q \geqslant 0 \, : \, \forall \, \delta > 0, \, \exists \, \text{a } \delta\text{-packing } \left(\mathcal{D}_j(\delta) \right)_{j \in J_{\mathcal{D}}} \text{ of } \mathcal{F} \text{ such that } \sum_{j \in J_{\mathcal{D}}} \delta^t \left(\mu \left(\mathcal{D}_j(\delta) \right)^q \right) \geqslant 1 \right\} ,$$

where the δ packing $\left(\mathcal{D}_j(\delta) \right)_{j \in J_{\mathcal{D}}}$ of $\mathcal{F}$, where $J_{\mathcal{D}} \subset \mathbb{N}$ is either finite or countably infinite, consists in a collection of pairwise disjoint disks $\mathcal{D}_j(\delta)$ of center $z_j \in \mathcal{D}_j$ and diameter $\delta_j \leqslant \delta$.

By comparison with classical methods, the computation relies on partitions of $\mathcal{F}$ into sets of equal measure, instead of sets of equal diameter.

As is explained in [Mak98], the usual choice for the entropy function consists in letting, for all $\delta > 0$, with associated grid of squares of the δ-coordinate mesh $\mathcal{G}(\delta) = \left(\mathcal{Q}_j(\delta) \right)_{j \in J_{\mathcal{Q}}}$, where $J_{\mathcal{Q}} \subset \mathbb{N}$ is either finite or countably infinite, and introducing the discrete partition function Z such that

$$S(q, \delta) = \sum_{\mathcal{Q}(\delta) \in \mathcal{G}(\delta), \, \mathcal{Q}(\delta) \cap \mathcal{F} \neq \varnothing} \left(\mu \left(\mathcal{Q}^\star(\delta) \right) \right)^q \quad ,$$

where, for each $\mathcal{Q}(\delta) \in \mathcal{G}(\delta)$, $\mathcal{Q}^\star(\delta)$ is the dilated cell obtained by means of the concentric enlargement of $\mathcal{Q}(\delta)$ by a fixed factor (here, 2) deduced from $\mathcal{Q}$. The underlying aim is to prevent boundary effects, while preserving the scaling law when $\delta \to 0^+$.

We are then looking for local scaling laws, where, for each possible value of the (local) scale $\alpha \geqslant \dfrac{1}{2}$, the number $\mathcal{N}(\alpha)$ of squares in $\mathcal{Q}$ such that

$$\mu \left(\mathcal{Q}(\delta) \right) \approx \delta^\alpha \, ,$$

is such that

$$\mathcal{N}(\alpha) \approx \delta^{-f(\alpha)} \, ,$$

which yields

$$S(q, \delta) \approx \sum_{\mathcal{Q}(\delta) \in \mathcal{G}(\delta), \, \mathcal{Q}(\delta) \cap \mathcal{F} \neq \varnothing} \delta^{\alpha \, q} \approx \sum_{\alpha} \mathcal{N}(\alpha) \, \delta^{\alpha \, q} \, ,$$

i.e.,

$$S(q, \delta) \approx \sum_{\alpha} \delta^{\alpha \, q - f(\alpha)} \, .$$

3.3 Constraints on the Multifractal Spectrum

Note that $\alpha \geqslant \dfrac{1}{2}$ – a lower bound which is not always explicitly written in the literature, as is the case in [Mak98] for the definition of the spectrum. This directly comes from the Beurling Projection Theorem, and its corollary, respectively given in Part III, Chapter 9, on pages 105 and 107, of [GM05], in the specific case when the measure μ is the harmonic measure ω: given a simply connected domain Ω, along with $z \in \Omega$ and $\zeta \in \partial\Omega$, then, for a sufficiently small real number r, the harmonic measure of the ball $\mathcal{B}(\zeta, r)$ of center ζ and radius r, viewed from the point z, is such that

$$\omega \left(z, \mathcal{B}(\zeta, r) \cap \partial\Omega, \Omega \right) \leqslant C \, r^{\frac{1}{2}} \, ,$$

where C is a strictly positive constant, which depends on Ω. Since we deal with small values of r (with associated negative logarithms), this result means that the harmonic measure decreases at most

like $r^{\frac{1}{2}}$, which calls for the universal lower bound $\alpha \geqslant \dfrac{1}{2}$ in our context.

There is also an upper bound $\alpha \leqslant \alpha_{\max}$, which directly comes from the fact that the map $\alpha \mapsto f(\alpha)$ is concave (see, for instance, [DB02]), and that the admissible values of α are precisely those corresponding to positive values of $f(\alpha)$; i.e.; the values for which the associated level sets are non-empty.

This ensures that the support of the universal spectrum $f(\alpha)$ is compact, of the form $\left[\dfrac{1}{2}, \alpha_{\max}\right]$, where $\alpha_{\max} \geqslant \dfrac{1}{2}$ is finite. This support coincides with the interval of possible values of the exponent α associated with the involved measure μ (which means, in particular, that, for all $\alpha \in \mathbb{R} \setminus \left[\dfrac{1}{2}, \alpha_{\max}\right]$, we either have that $f(\alpha) \leqslant 0$ or $f(\alpha) = -\infty$).

We set

$$\tau(q) = \limsup_{\delta \to 0^+} \frac{\ln S(q,\delta)}{|\ln \delta|} .$$

For sufficiently small values of the diameter δ, a standard Laplace (saddle-point) asymptotic estimate of the integral as $\delta \to 0^+$ enables us to obtain that

$$S(q,\delta) \approx \int_{\frac{1}{2}}^{\alpha_{\max}} \delta^{\alpha q - f(\alpha)} \, d\alpha \approx \delta^{\sup_{\frac{1}{2} \leqslant \alpha \leqslant \alpha_{\max}} [f(\alpha) - \alpha q]} .$$

By applying the Legendre transformation, we deduce that

$$-\tau(q) = \inf_{\frac{1}{2} \leqslant \alpha \leqslant \alpha_{\max}} (\alpha q - f(\alpha)) .$$

The multifractal spectrum can then be obtained by applying the inverse Legendre transformation,

$$f(\alpha) = \inf_{q \in \mathbb{R}} (\alpha q - \tau(q)) .$$

Remark 3.1 (**From Disks to Squares in the Makarov Setting – A Road to the Numerical Implementation**).

An interesting comment can be made about the implicit transition from the initial δ-packing $\left(\mathcal{D}_j\right)_{j \in J}$ of $\mathcal{F}$, consisting of disjoint disks, in the Makarov setting recalled above, immediately followed by a mesh $\mathcal{Q}$ this time consisting of squares. At small scales, not only are squares and disks comparable – in terms of associated scaling exponents – also, when computations come into the play, the use of squares is much better, insofar as it enables us to obtain nested packings, i.e., packings with a regular and natural hierarchy of boxes (each square can be divided into smaller squares), contrary to packings involving disks, inherently unnested, as they do not admit a natural hierarchical subdivision.

In terms of the computation of $\tau(q) = \limsup_{\delta \to 0^+} \dfrac{\ln S(q,\delta)}{|\ln \delta|}$, which is simply a linear regression in $\ln S(q,\delta)$ over $|\ln \delta|$, we clearly see that a nested packing will result in a progressive growth as a function of δ, with quasi-linear variations and, hence, a stable slope, which is again much better in the light of the Legendre transform.

By comparison, in the case of an unnested packing of disks, each variation in scales involves a completely new family of disks, which can result in potentially high variations in $\ln S(q,\delta)$ when δ decreases (or when $|\ln \delta|$ increases). The slope can thus be subjected to noises.

3.4 Multiscale Structure induced by the Weierstrass Driving Function

Hereafter, we emphasize the specific features of the Weierstrass-driven case. Indeed, the multiscale structure of the driving function induces a hierarchy of oscillations, which directly affects the distribution of the local scaling exponents α.

In practice, based upon the above comments in Remark 3.1, the computation of the universal multifractal spectrum $f(\alpha)$ can be numerically implemented by using the method given by Ashvin Chhabra and Roderick V. Jensen in [CJ89]. The method, which, a priori surprisingly, does not involve the use of the Legendre transform, relies on δ-packings (where $\delta > 0$) which, of course, consists in a family of squares $\mathcal{Q}(\delta) = \big(\mathcal{Q}_j(\delta)\big)_{j \in J_{\mathcal{Q}}}$, of side-length equal to δ. Note that, unlike in Makarov's definition for the entropy function, where dilated cells are involved in order to handle boundary effects, the Chhabra–Jensen method directly relies on the original grid cells; no significant boundary effects are expected. We then introduce, still for all $\delta > 0$ and for all $q \geqslant 0$, a two-parameters family $\big(\mu_j\big)_{j \in J_{\mathcal{Q}}}$ of normalized measures which depend on q and δ and are such that, for each $j \in J_{\mathcal{Q}}$,

$$\mu_j\,(q,\delta) = \frac{\big(\mu\,(\mathcal{Q}_j)\big)^q}{\displaystyle\sum_{k \in J_{\mathcal{Q}}} \big(\mu\,(\mathcal{Q}_k)\big)^q}\,.$$

We thus have at our disposal a probability measure on the mesh $\mathcal{Q}$.

We then introduce

$$\alpha(q) = \lim_{\delta \to 0^+} \sum_{j \in J_{\mathcal{Q}}} \frac{\mu_j\,(\mathcal{Q},\delta)\,\ln\big(\mu\,(\mathcal{Q}_j)\big)}{\ln \delta}\,,$$

along with

$$f(q) = \lim_{\delta \to 0^+} \sum_{j \in J_{\mathcal{Q}}} \frac{\mu_j\,(\mathcal{Q},\delta)\,\ln\big(\mu_j\,(q,\delta)\big)}{\ln \delta}\,.$$

Note that, again unlike Makarov's formalism recalled just above, the respective expressions for $\alpha(q)$ and $f(q)$ are obtained by means of limits taken in the usual sense, instead of lim sup. In Makarov's setting, this reflects the fact that for the involved measure, the limit may fail to exist due to oscillations occurring at different scales. By contrast, in the Chhabra–Jensen perspective, the measure is computed on regular dyadic grids, for which these limits are known to exist in a large class of cases, such as Gibbs measures (see, for instance, Theorem II. 5, on page 95, in the paper by Yakov Pesin and Howard Weiss [PW97]), or self-similar measures (see, in particular, Equation 17. 37 of Lemma 17. 5, in Section 17 of Kenneth Falconer's book [Fal14]).

For all $q \geqslant 0$, $\alpha(q)$ is referred to as *an average singularity strength*, while $f(q)$ represents the fractal dimension of the mesh boxes with singularity $\alpha(q)$.

Therefore, the sought for multifractal universal spectrum is then obtained by plotting the parametrized curve $(\alpha(q), f(q))$.

Our computations rely on the use of the normalized counting measure supported on the discrete trace, where each point of the polygonal curve contributes equally. This ensures that the measure of each box involved is proportional to the number of points belonging to the trace located in this box.

The corresponding plots, in the case of Weierstrass prefractal driven hulls, in the case when $\lambda = \frac{1}{\sqrt{2}}$, $N_b = 2$, $N = 7$, $N = 8$, $N = 10$, are displayed in Figures 8. We note that the spectra obtained for $N = 7$ and $N = 8$ are very close. A noticeable change can be observed in the case $N = 10$, which shows that the geometry of the hull changes when the polygonal depth N increases, which reflects the fact that an increase in N is synonymous with involving more and more finer scales in the drift, resulting with

more and more singularities in the hull (see Figures 6 and Figures 5). The polygonal depth N is, therefore, both an indicator of the roughness of the drift and of the resulting hull. We do not display the plot corresponding to higher values of N, which have small loops due to finite-resolution effects.

We stress the fact that the displayed spectra correspond to a Weierstrass prefractal drift, and not to a Weierstrass-truncated drift, where the hulls remain comparatively smooth. Increasing the order of the approximation does not lead to a significant evolution of the spectrum. In addition, since the Weierstrass-truncated drift has finitely many frequencies, increasing the order of the approximation does not intrinsically change the geometry, as it can be observed in Figure 10 and Figure 11.

In summary, the polygonal depth N controls the appearance of new scales both in the drift and in the resulting hull. This highlights a fundamental connection between the regularity of the drift and the geometric complexity of the trace. This observation is consistent with the classical growth and distortion estimates (see, for instance, [GM05], Theorem 4. 5, on page 22) coming from Koebe's (distortion) Theorem (see also [GM05]), Theorem 4. 3, on page 19), which states that, given a conformal, univalent map ψ such that $\psi(0) = 0$ and $\psi(1) = 1$, then, for all $z \in \mathbb{C}$,

$$\frac{|z|}{(1+|z|)^2} \leqslant |\psi(z)| \leqslant \frac{|z|}{(1-|z|)^2}\,,$$

along with

$$\frac{1-|z|}{(1+|z|)^3} \leqslant |\psi'(z)| \leqslant \frac{1+|z|}{(1-|z|)^3}\,.$$

In our present context, this means that the small oscillations of the (Weierstrass prefractal) drift lead to oscillations of the hull.

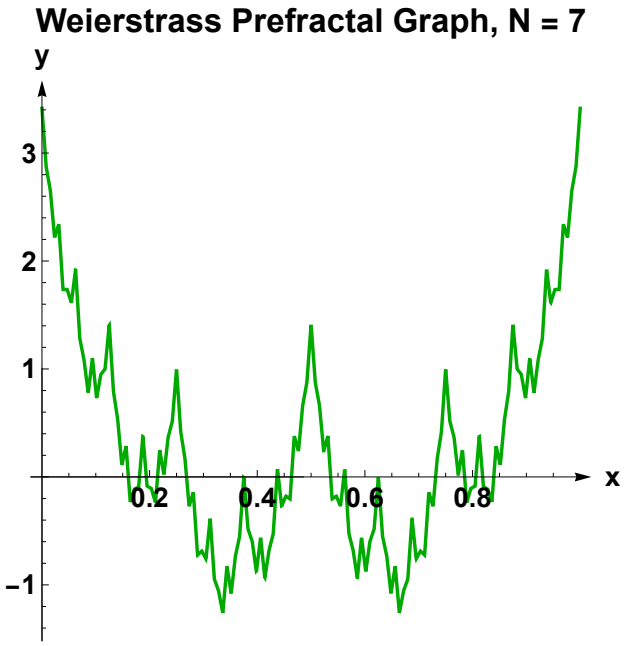

(a) The Weierstrass prefractal graph, for $\lambda = \frac{1}{\sqrt{2}}$, $N_b = 2$, $N = 7$.

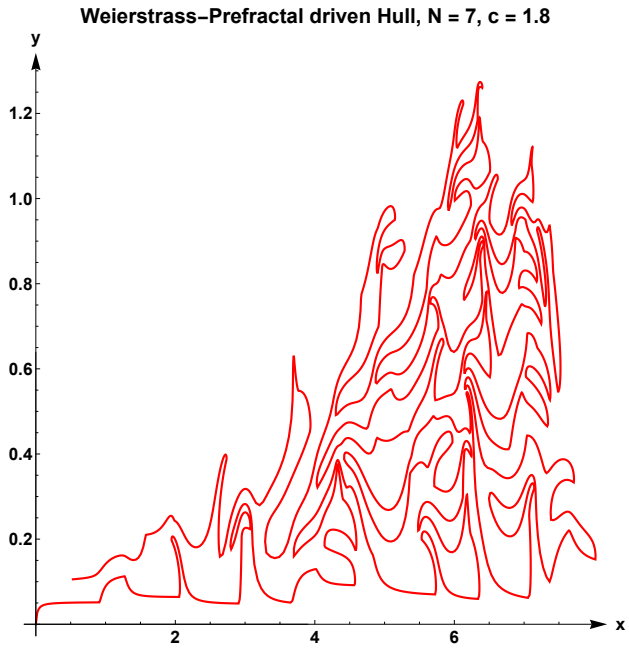

(b) The Weierstrass prefractal driven hull, for $\lambda = \frac{1}{\sqrt{2}}$, $N_b = 2$, $N = 7$, $c = 1.8$.

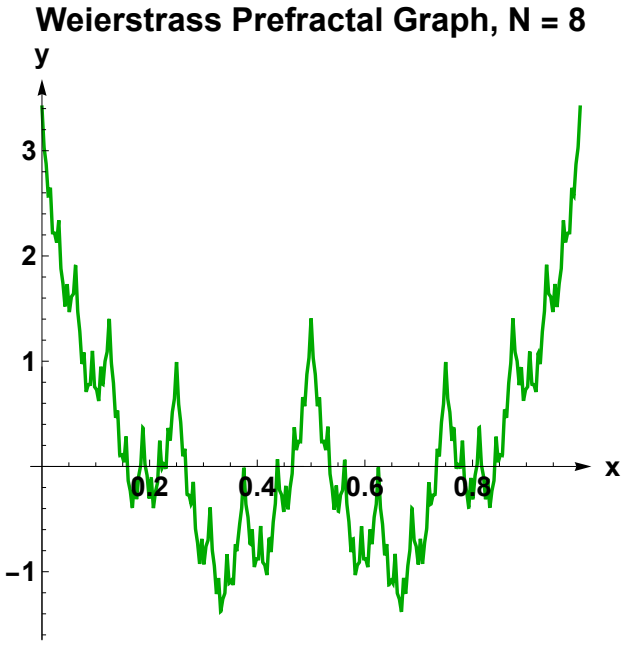

(c) The Weierstrass prefractal graph, for $\lambda = \frac{1}{\sqrt{2}}$, $N_b = 2$, $N = 8$.

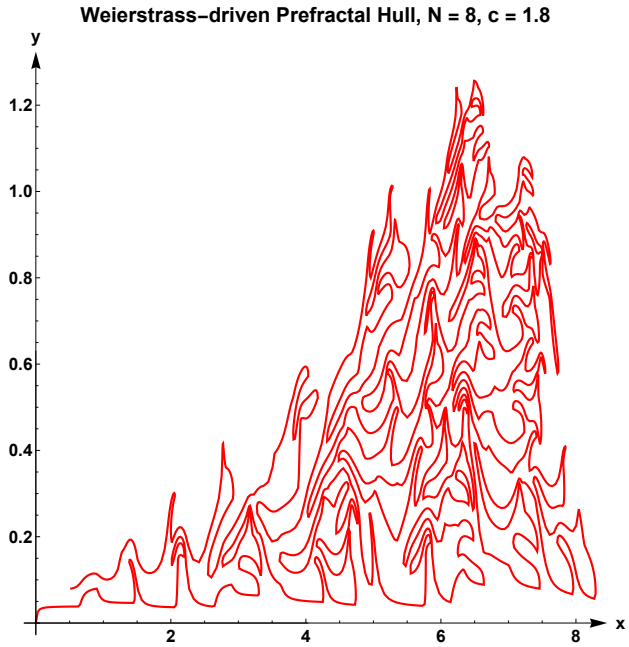

(d) The Weierstrass prefractal driven hull, for $\lambda = \frac{1}{\sqrt{2}}$, $N_b = 2$, $N = 8$, $c = 1.8$.

Figure 4: **The Weierstrass prefractal graphs, and the Weierstrass-prefractal driven hulls, in the case when $\lambda = \frac{1}{\sqrt{2}}$, $N_b = 2$, $N \in \{7, 8\}$, $c = 1.8$. The driving function has been computed by means of a linear interpolation between a uniformly distributed sequence of points belonging to the Weierstrass Curve. This polygonal approximation is suited to a stable and efficient integration in the Marshall and Rohde algorithm, while preserving the main properties of the intended drift (the Weierstrass function). The hull displays an almost self-similarity and a noticeable roughness, coherent with the fractal nature of the drift.**

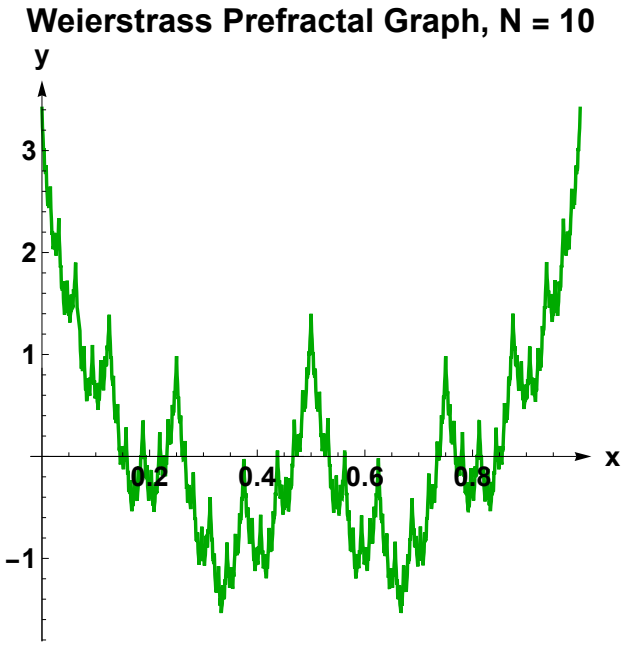

(a) The Weierstrass prefractal graph, for $\lambda = \frac{1}{\sqrt{2}}$, $N_b = 2$, $N = 10$.

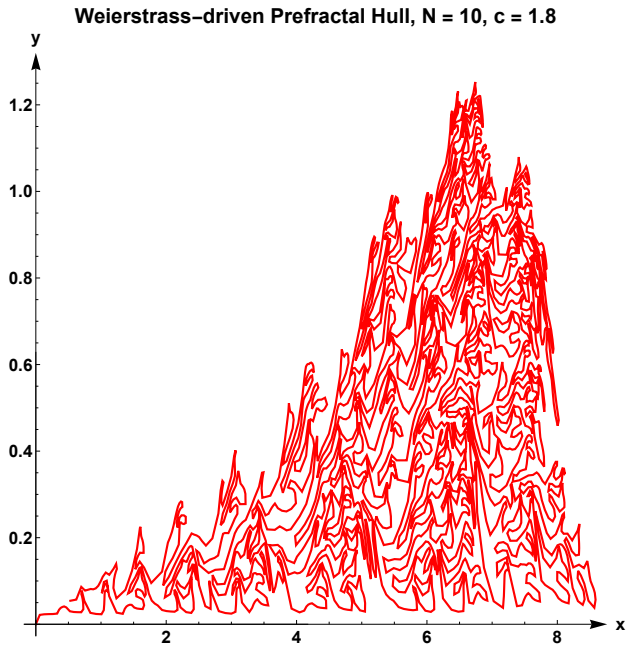

(b) The Weierstrass prefractal graph, for $\lambda = \frac{1}{\sqrt{2}}$, $N_b = 2$, $N = 10$, $c = 1.8$.

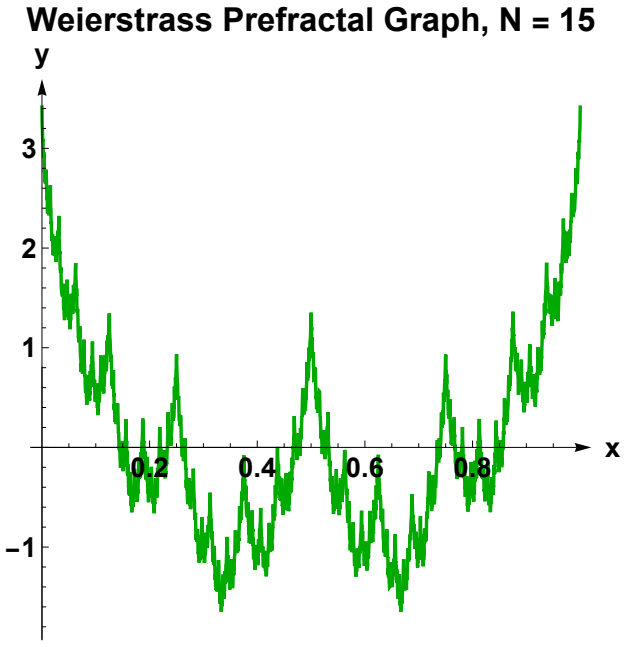

(c) The Weierstrass prefractal graph, for $\lambda = \frac{1}{\sqrt{2}}$, $N_b = 2$, $N = 15$.

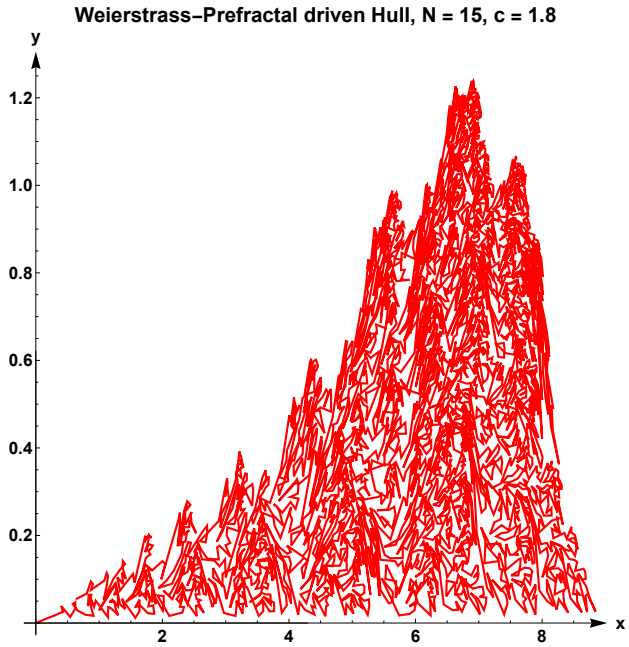

(d) The Weierstrass prefractal driven hull, for $\lambda = \frac{1}{\sqrt{2}}$, $N_b = 2$, $N = 15$, $c = 1.8$.

Figure 5: **The Weierstrass prefractal graphs, and the Weierstrass prefractal driven hulls, in the case when $\lambda = \frac{1}{\sqrt{2}}$, $N_b = 2$, $N \in \{10, 15\}$, $c = 1.8$. The driving function has been computed by means of a linear interpolation between a uniformly distributed sequence of points belonging to the Weierstrass Curve. This polygonal approximation is suited to a stable and efficient integration in the Marshall and Rohde algorithm, while preserving the main properties of the intended drift (the Weierstrass function). The hull displays an almost self-similarity and a noticeable roughness, coherent with the fractal nature of the drift.**

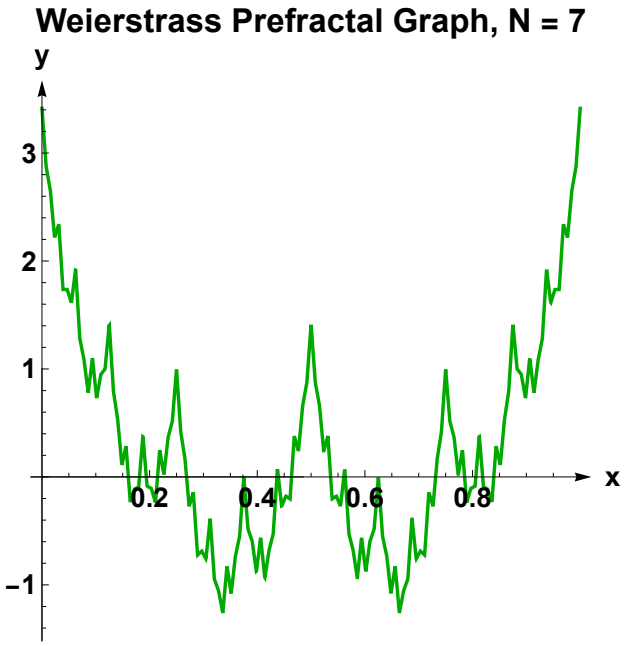

(a) The Weierstrass prefractal graph, for $\lambda = \frac{1}{\sqrt{2}}$, $N_b = 2$, $N = 7$.

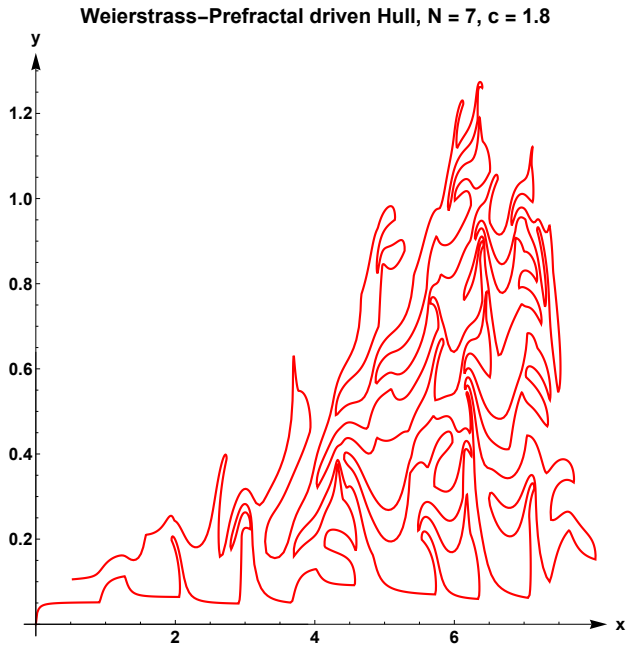

(b) The Weierstrass prefractal driven hull, for $\lambda = \frac{1}{\sqrt{2}}$, $N_b = 2$, $N = 7$, $c = 1.8$.

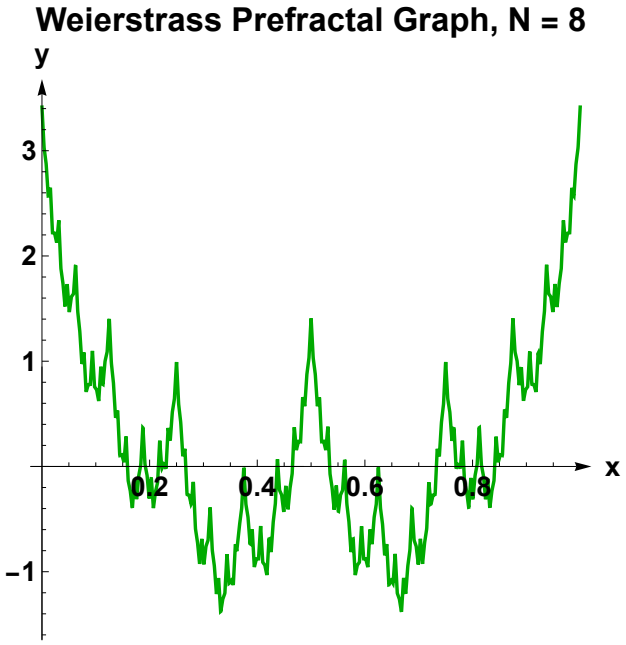

(c) The Weierstrass prefractal graph, for $\lambda = \frac{1}{\sqrt{2}}$, $N_b = 2$, $N = 8$.

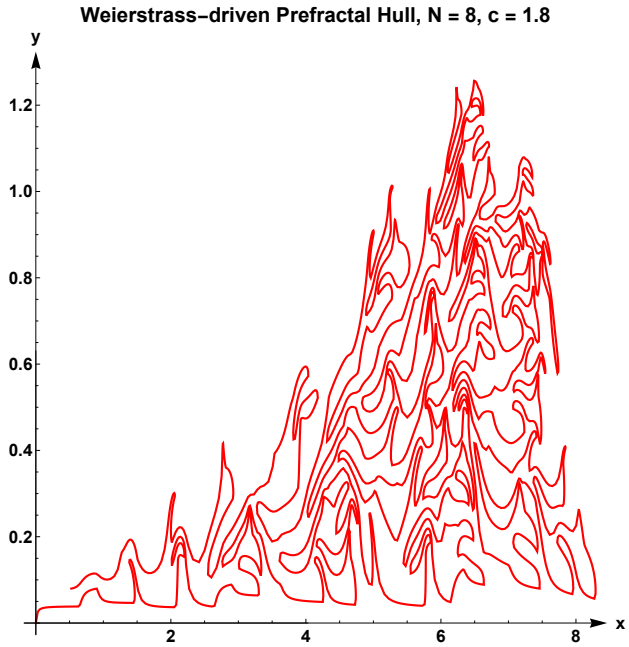

(d) The Weierstrass prefractal driven hull, for $\lambda = \frac{1}{\sqrt{2}}$, $N_b = 2$, $N = 8$, $c = 1.8$.

Figure 6: **The Weierstrass prefractal graphs, and the Weierstrass-prefractal driven hulls, in the case when $\lambda = \frac{1}{\sqrt{2}}$, $N_b = 2$, $N \in \{7, 8\}$, $c = 1.8$. The driving function has been computed by means of a linear interpolation between a uniformly distributed sequence of points belonging to the Weierstrass Curve. This polygonal approximation is suited to a stable and efficient integration in the Marshall and Rohde algorithm, while preserving the main properties of the intended drift (the Weierstrass function). The hull displays an almost self-similarity and a noticeable roughness, coherent with the fractal nature of the drift.**

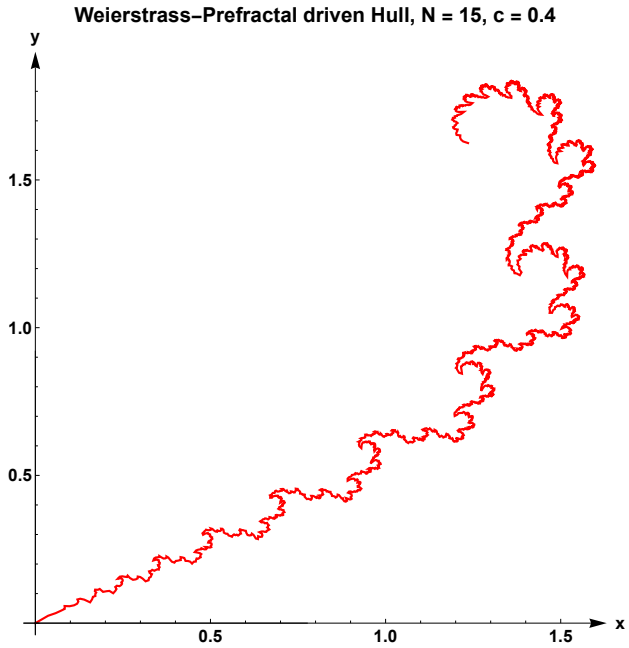

(a) **The Weierstrass prefractal driven hull, for $\lambda = \frac{1}{\sqrt{2}}$, $N_b = 2$, $N = 15$, $c = 0.4$.**

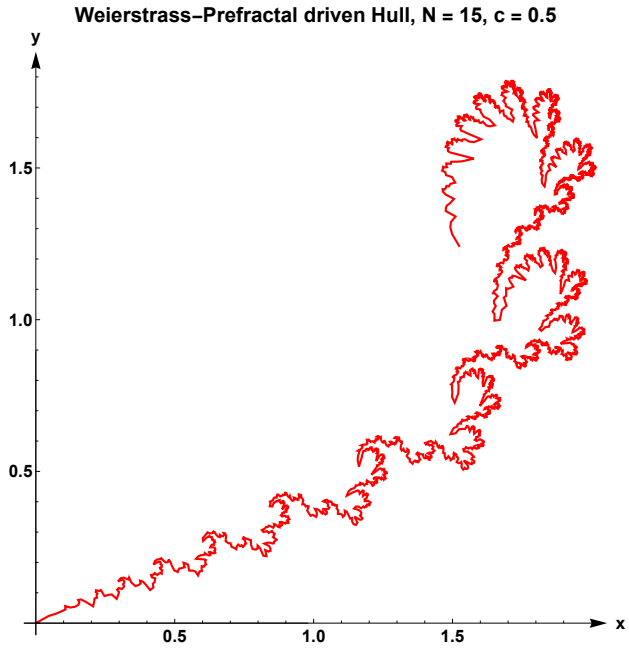

(b) **The Weierstrass prefractal driven hull, for $\lambda = \frac{1}{\sqrt{2}}$, $N_b = 2$, $N = 15$, $c = 0.5$.**

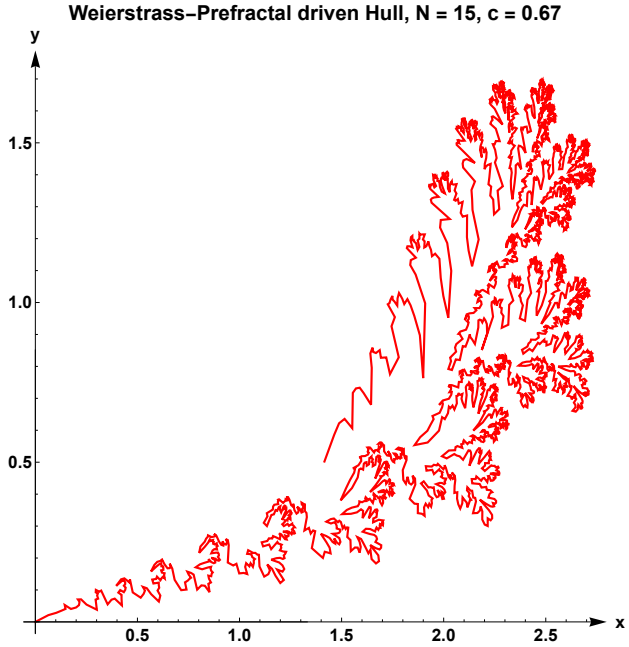

(c) **The Weierstrass prefractal driven hull, for $\lambda = \frac{1}{\sqrt{2}}$, $N_b = 2$, $N = 15$, $c = 0.672$.**

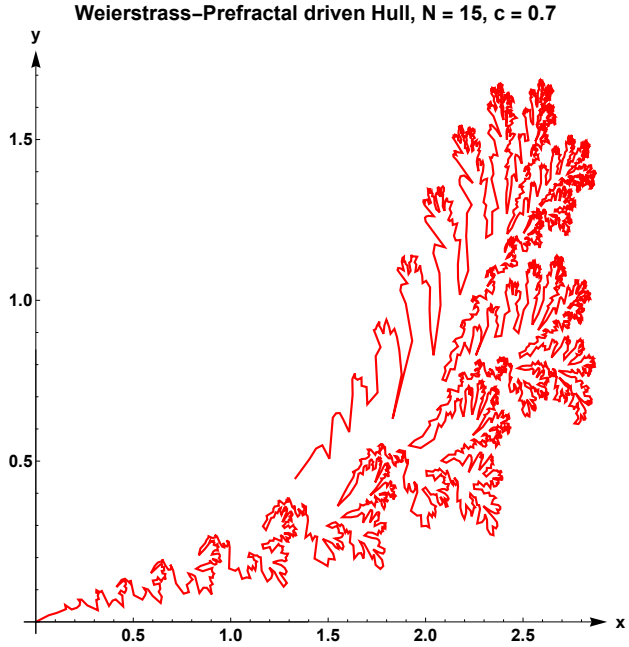

(d) **The Weierstrass prefractal driven hull, for $\lambda = \frac{1}{\sqrt{2}}$, $N_b = 2$, $N = 15$, $c = 0.7$.**

Figure 7: **The phase transition, in the case of Weierstrass-prefractal driven hulls, when $\lambda = \dfrac{1}{\sqrt{2}}$, $N_b = 2$, $N = 15$.**

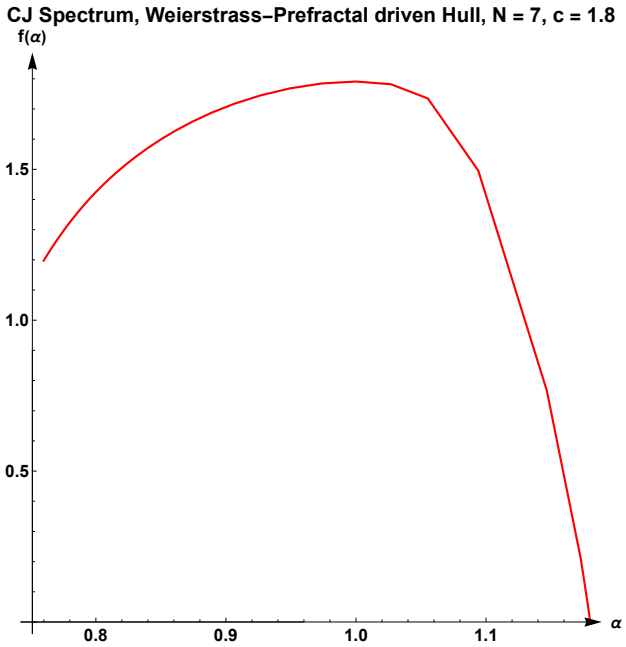

(a) **The Chhabra–Jensen (CJ) multifractal spectrum of the Weierstrass prefractal driven hull, for $\lambda = \frac{1}{\sqrt{2}}$, $N_b = 2$, $N = 7$, $c = 1.8$.**

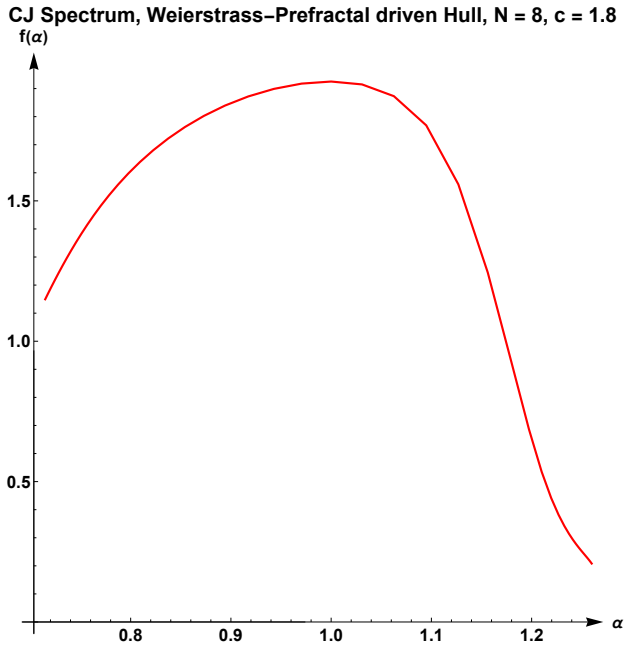

(b) **The Chhabra–Jensen (CJ) multifractal spectrum of the Weierstrass prefractal driven hull, for $\lambda = \frac{1}{\sqrt{2}}$, $N_b = 2$, $N = 8$, $c = 1.8$.**

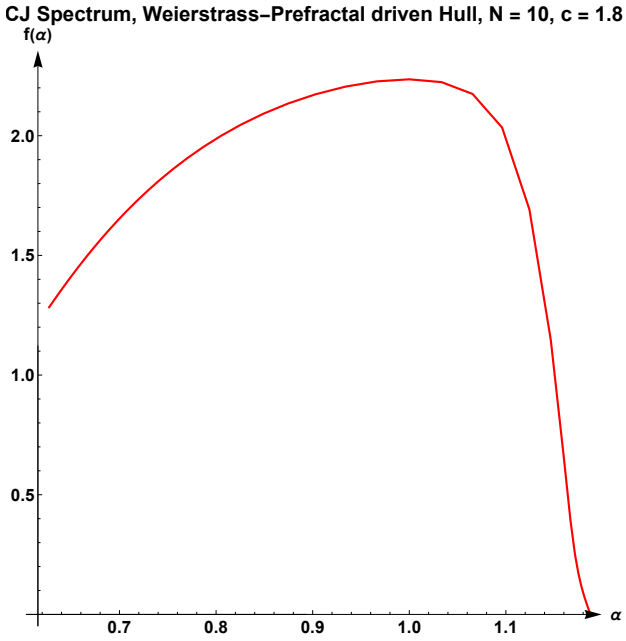

(c) **The Chhabra–Jensen (CJ) multifractal spectrum of the Weierstrass prefractal driven hull, for $\lambda = \frac{1}{\sqrt{2}}$, $N_b = 2$, $N = 10$, $c = 1.8$.**

Figure 8: **The Chhabra–Jensen (CJ) multifractal spectra of the Weierstrass-prefractal driven hulls, in the case when $\lambda = \frac{1}{\sqrt{2}}$, $N_b = 2$, $N \in \{7, 8, 10\}$, $c = 1.8$.**

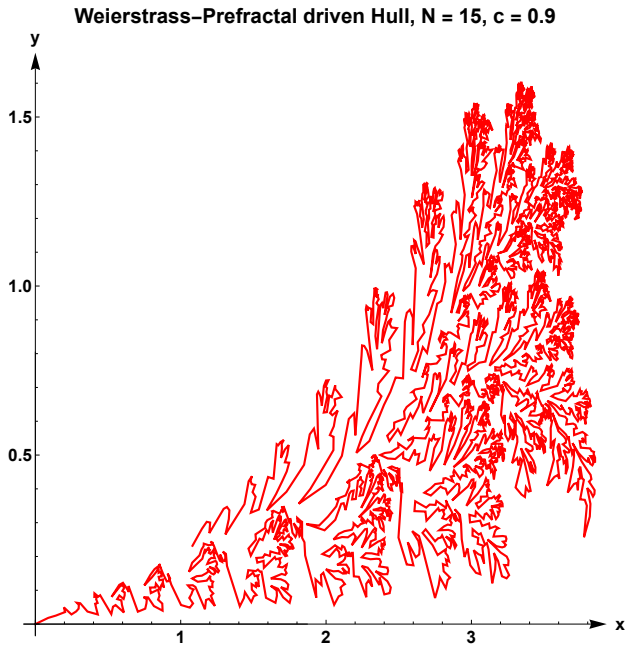

(a) **The Weierstrass prefractal driven hull, for $\lambda = \frac{1}{\sqrt{2}}$, $N_b = 2$, $N = 15$, $c = 0.9$.**

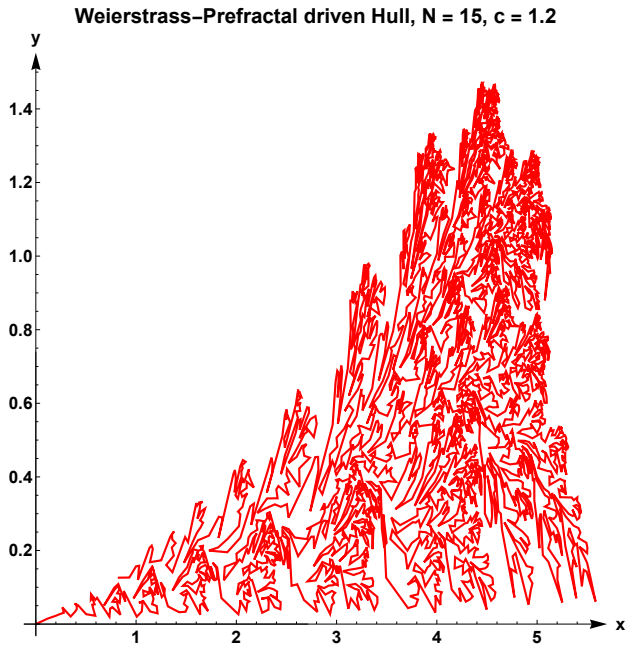

(b) **The Weierstrass prefractal driven hull, for $\lambda = \frac{1}{\sqrt{2}}$, $N_b = 2$, $N = 15$, $c = 1.2$.**

Figure 9: **The phase transition (from simple to nonsimple curves), in the case of Weierstrass-prefractal driven hulls, when $\lambda = \dfrac{1}{\sqrt{2}}$, $N_b = 2$, $N = 15$.**

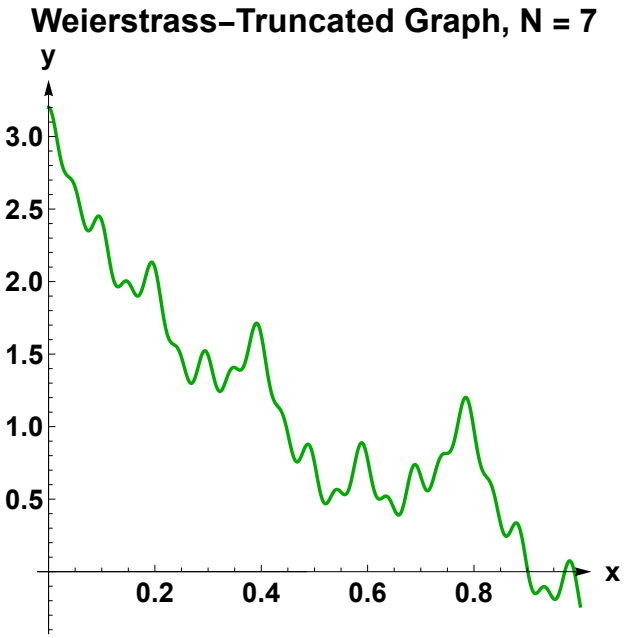

(a) The Weierstrass truncated graph, for $\lambda = \frac{1}{\sqrt{2}}$, $N_b = 2$, $N = 7$.

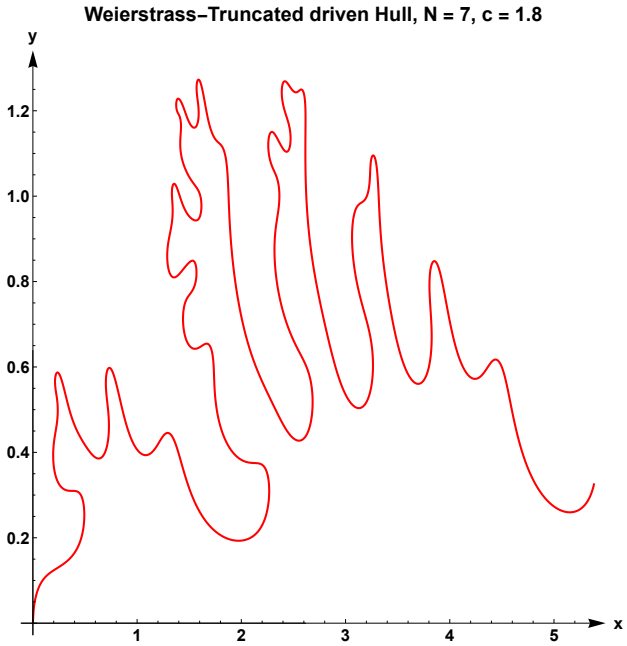

(b) The Weierstrass truncated driven hull, for $\lambda = \frac{1}{\sqrt{2}}$, $N_b = 2$, $N = 7$, $c = 1.8$.

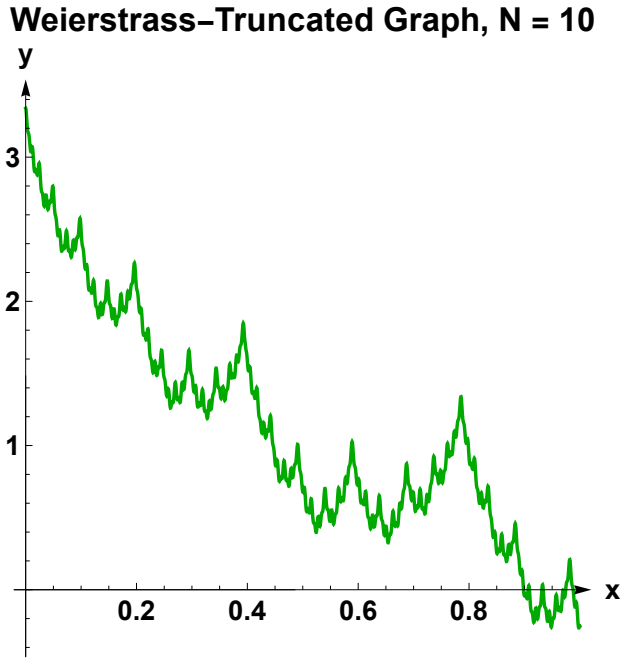

(c) The Weierstrass truncated graph, for $\lambda = \frac{1}{\sqrt{2}}$, $N_b = 2$, $N = 10$.

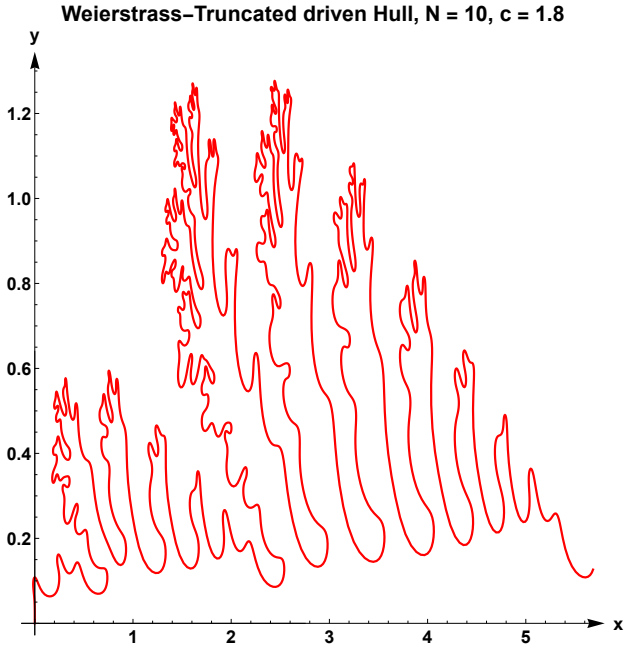

(d) The Weierstrass truncated driven hull, for $\lambda = \frac{1}{\sqrt{2}}$, $N_b = 2$, $N = 10$, $c = 1.8$.

Figure 10: **The Weierstrass-truncated graphs, and the Weierstrass-truncated hulls, in the case when $\lambda = \frac{1}{\sqrt{2}}$, $N_b = 2$, $N \in \{7, 10\}$, $c = 1.8$. When N increases, the drift becomes more and more irregular, and so does the resulting hull.**

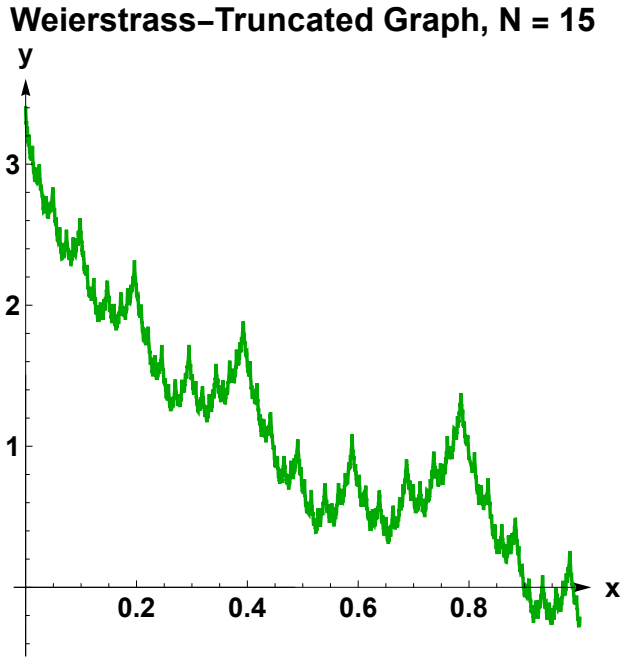

(a) **The Weierstrass truncated graph, for $\lambda = \frac{1}{\sqrt{2}}$, $N_b = 2$, $N = 15$.**

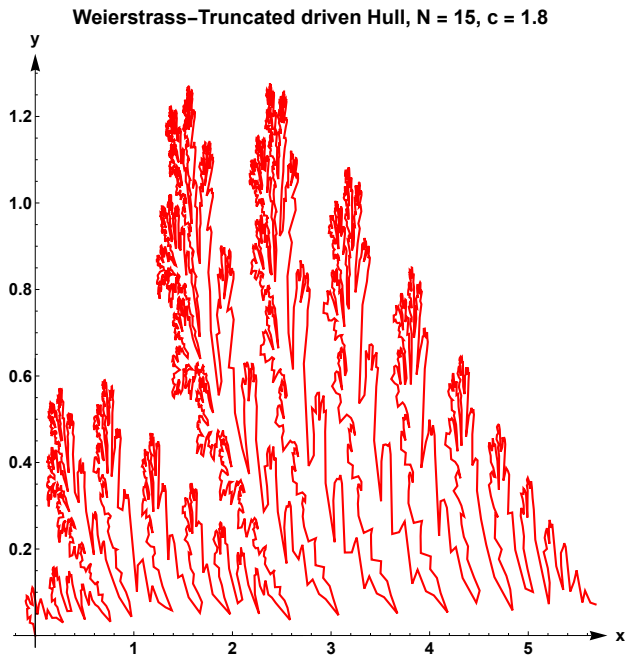

(b) **The Weierstrass truncated driven hull, for $\lambda = \frac{1}{\sqrt{2}}$, $N_b = 2$, $N = 15$, $c = 1.8$.**

Figure 11: **The Weierstrass-truncated graphs, and the Weierstrass-truncated hulls, in the case when $\lambda = \dfrac{1}{\sqrt{2}}$, $N_b = 2$, $N = 15$, $c = 1.8$. When N increases, the drift becomes more and more irregular, and so does the resulting hull.**

Some additional comments relative to the figures displayed in [Lin05], on page 153, in the case when $\lambda = \dfrac{1}{\sqrt{2}}$ and $N_b = 2$ are as follows. We were interested both in reproducing those plots, for which neither a method nor an algorithm was given, and in obtaining plots associated with different parameters λ and N_b for the Weierstrass drift. As previously, we have used the method given by Huy Tran in [Tra15].

Our results, obtained with *Mathematica* (Wolfram), are displayed in Figure 12, on page 37, and in Figure 14, on page 39.

We note that our hulls display a *quasi self-simillarity*, in the sense that if we zoom (see Figure 13), we distinguish patterns of the same type as the ones that appear on the whole hull, as is the case for the Weierstrass Curve, where there is a correspondance between patterns (polygons) between consecutive scales; see, for instance, [DL24c], [DL25d], [DL25b], [DL25a]. In the light of the self-affinity – and the fractality – of the Brownian motion, this suggests a possible connection between the intrinsic properties of the drift, and the resulting traces.

In [Lin05], Figure 2, on page 153, the authors display the plots obtained for the SLE hulls in the case of a Weierstrass drift, with associated parameters $\lambda = \dfrac{1}{\sqrt{2}}$ and $N_b = 2$. We have numerically computed the box-counting dimensions associated with their plots. Our values are displayed in Table 3, on page 36.

We note that the numerical values for the box-counting dimensions increase from 1.32063 (in the case when $c = 0.8$) to 1.50547 (in the case when $c = 1.8$). This latter value is very close to the box-counting dimension of the Weierstrass Curve in the case when $\lambda = \dfrac{1}{\sqrt{2}}$ and $N_b = 2$, which is

$$2 - \frac{\ln \lambda}{\ln N_b} = 1.5\,.$$

Insofar as the box-counting (or Minkoswki) dimension of the Weierstrass Curve is, also, the abscissa of convergence of the global fractal zeta function associated with the Weierstrass Curve (see our previous works [DL25d], [DL25b]), we therefore wonder whether there are underlying connections between the Weierstrass drift, and the corresponding SLE trace/hull. Thus far, we do not have at our disposal relevant theoretical results. However, we conjecture a correspondence between the (global) fractal zeta function associated with a Weierstrass drift, and the (global) fractal zeta function associated with the corresponding SLE trace.

$\boldsymbol{c}$	0.8	1	1.2	1.4	1.6	1.8
Box-counting dimension	1.32063	1.41734	1.4795	1.53176	1.56758	1.50547

Table 3: Computed box-counting dimensions associated with the SLE traces displayed in [Lin05], Figure 2, on page 153.

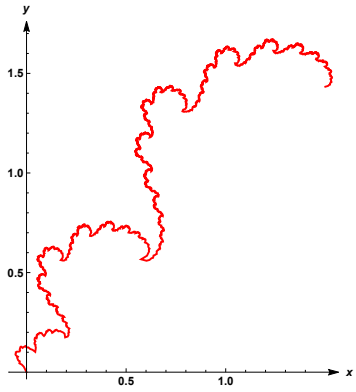

(a) **The Weierstrass-truncated driven hull, in the case when $\lambda = \frac{1}{\sqrt{2}}$, $N_b = 2$, $c = 0.8$; computation of 15,000 steps.**

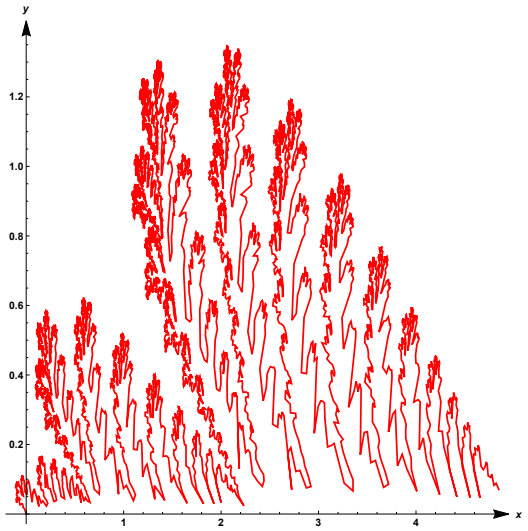

(b) **The Weierstrass-truncated driven hull, in the case when $\lambda = \frac{1}{\sqrt{2}}$, $N_b = 2$, $c = 1.6$; computation of 15,000 steps.**

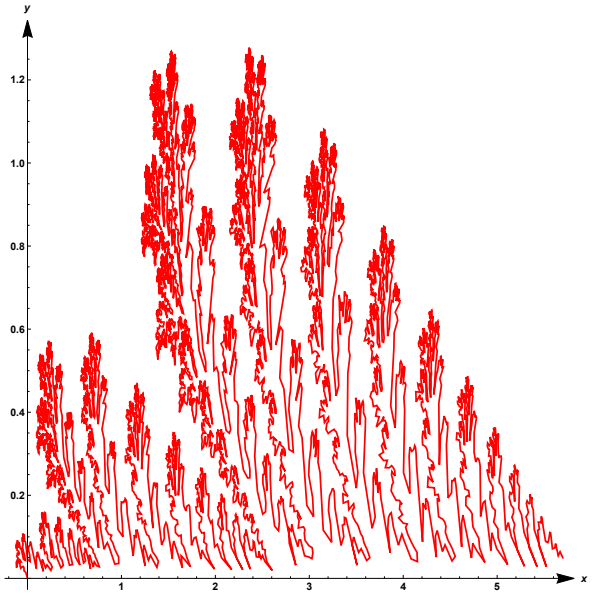

(c) **The Weierstrass-truncated driven hull,in the case when $\lambda = \frac{1}{\sqrt{2}}$, $N_b = 2$, $c = 1.8$; computation of 15,000 steps.**

Figure 12: **The Weierstrass-truncated driven hulls, in the case when $\lambda = \frac{1}{\sqrt{2}}$, $N_b = 2$, $c \in \{0.8, 1.6, 1.8\}$.**

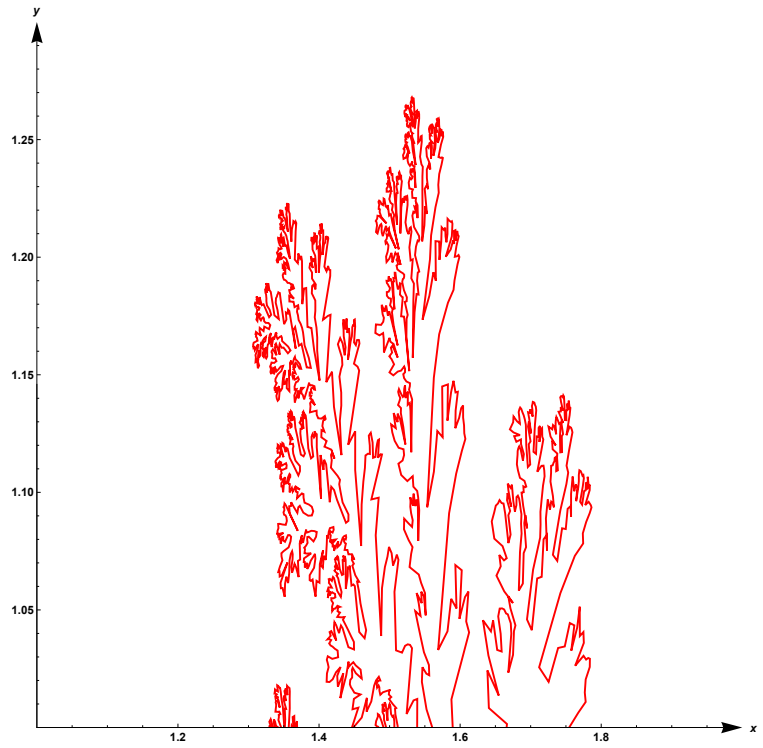

Figure 13: **A zoom of the Weierstrass-truncated driven hull, in the case when** $\lambda = \dfrac{1}{\sqrt{2}}$, $N_b = 2$, $c = 1.8$**; computation of** $15,000$ **steps.**

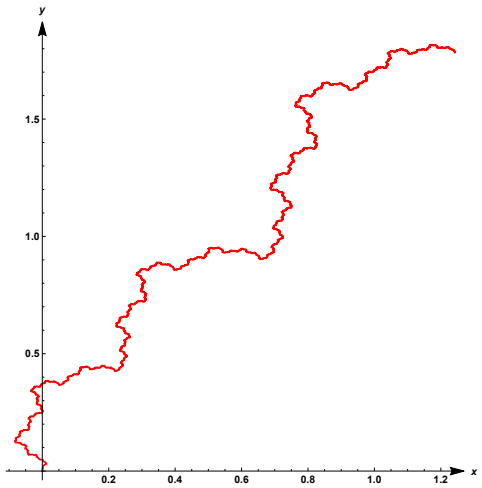

(a) **The Weierstrass-truncated driven hull, in the case when $\lambda = \frac{1}{\sqrt{3}}$, $N_b = 3$, $c = 0.8$, and $N = 15000$.**

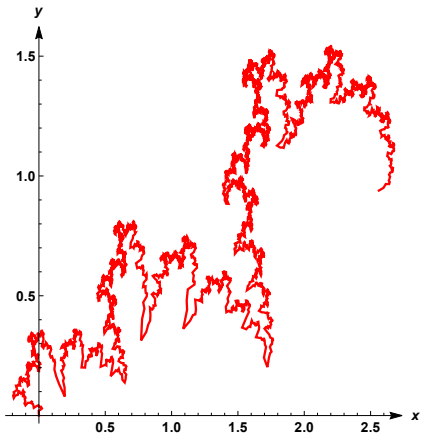

(b) **The Weierstrass-truncated driven hull, in the case when $\lambda = \frac{1}{\sqrt{3}}$, $N_b = 3$, $c = 1.6$, and $N = 10000$.**

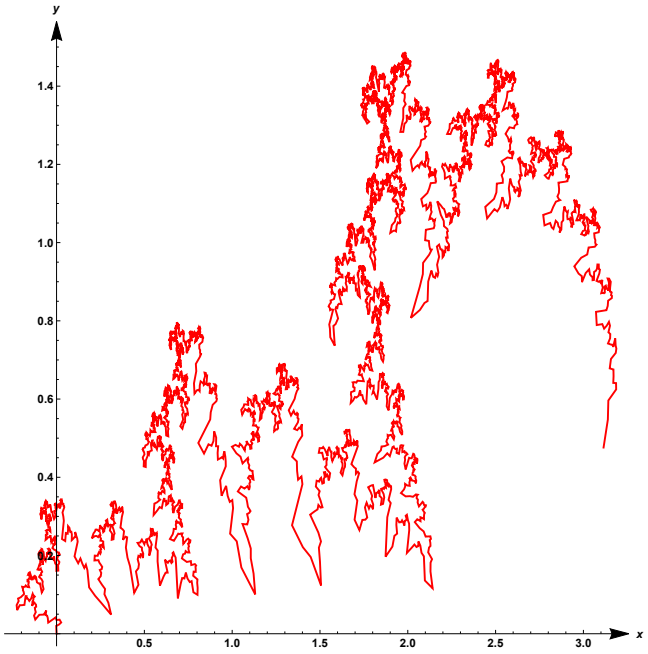

(c) **The Weierstrass-truncated driven hull, in the case when $\lambda = \frac{1}{\sqrt{3}}$, $N_b = 3$, $c = 1.8$, and $N = 10000$.**

Figure 14: **The Weierstrass-truncated driven hulls, in the case when $\lambda = \frac{1}{\sqrt{3}}$, $N_b = 3$, $c \in \{0.8, 1.6, 1.8\}$.**

4 Concluding Comments – Open Problems and Perspectives

Loewner traces driven by Weierstrass prefractal or truncated functions, playing the part of deterministic toy models for rough drivers, display fundamental connections with the geometry of the drift, which is more significant in the case of Weierstrass prefractal drifts. More precisely, the Chhabra–Jensen multifractal spectrum of the resulting trace broadens and reveals new scales when the polygonal depth of the drift increases. This reflects the corresponding geometric complexity of the hull. By comparison, Weierstrass-truncated drifts which, by nature, involve fewer scales and are smooth functions, generate smoother hulls. This numerical evidence, in agreement with classical distortion estimates (coming from Koebe's Distortion Theorem) supports the idea that the Weierstrass prefractal function is a well-suited deterministic toy model for studying the rough dynamics of the Loewner equation. The extension to other deterministic Weierstrass-type functions with controlled regularity (including the Takagi function, Knopp-type functions) will be the subject of future work.

Finally, the conformal context of SLE_κ, together with the results obtained above, raises the following question: can we establish a connection between the (fractal) complex dimensions (and the associated fractal zeta functions; see [DL25b], [DL25d]) of a fractal drift, such as a Weierstrass function, and the resulting fractal SLE traces?

This perspective suggests that deterministic fractal drivers, such as the Weierstrass function, may offer a new framework for investigating the geometric and multifractal structure of Loewner evolutions, complementing the classical probabilistic approach based on Brownian motion.

References

[Bar98] Martin T. Barlow. Diffusions on fractals. In *Lectures on Probability Theory and Statistics (Saint-Flour, 1995)*, volume 1690 of *Lecture Notes in Math.*, pages 1–121. Springer, Berlin, 1998. URL: https://doi.org/10.1007/BFb0092537.

[BBR14] Krzysztof Barański, Balázs Bárány, and Julia Romanowska. On the dimension of the graph of the classical Weierstrass function. *Advances in Mathematics*, 265:791–800, 2014.

[Bef08] Vincent Beffara. The dimension of the SLE curves. *The Annals of Probability*, 36(4):1421 – 1452, 2008. URL: https://doi.org/10.1214/07-AOP364.

[BP17] Christopher J. Bishop and Yuval Peres. *Fractals in Probability and Analysis*, volume 162 of *Cambridge Studies in Advanced Mathematics*. Cambridge University Press, Cambridge, 2017. URL: https://doi.org/10.1017/9781316460238.

[CJ89] Ashvin Chhabra and Roderick V. Jensen. Direct determination of the $f(\alpha)$ singularity spectrum. *Physical Review Letters*, 62(12):1327–1330, 1989. URL: https://doi.org/10.1103/PhysRevLett.62.1327.

[Dav18] Claire David. Bypassing dynamical systems: A simple way to get the box-counting dimension of the graph of the Weierstrass function. *Proceedings of the International Geometry Center*, 11(2):1–16, 2018. URL: https://journals.onaft.edu.ua/index.php/geometry/article/view/1028.

[Dav19] Claire David. On fractal properties of Weierstrass-type functions. *Proceedings of the International Geometry Center*, 12(2):43–61, 2019. URL: https://journals.onaft.edu.ua/index.php/geometry/article/view/1485.

[DB02] Bertrand Duplantier and Ilia A. Binder. Harmonic measure and winding of conformally invariant curves. *Physical Review Letters*, 89:264101, Dec 2002. URL: https://link.aps.org/doi/10.1103/PhysRevLett.89.264101.

[DB08] Bertrand Duplantier and Ilia A. Binder. Harmonic measure and winding of random conformal paths: a Coulomb gas perspective. *Nuclear Physics. B. Theoretical, Phenomenological, and Experimental High Energy Physics. Quantum Field Theory and Statistical Systems*, 802(3):494–513, 2008. URL: https://doi.org/10.1016/j.nuclphysb.2008.05.020.

[DL24a] Claire David and Michel L. Lapidus. Fractal complex dimensions and cohomology of the Weierstrass curve. In Patricia Alonso Ruiz, Michael Hinz, Kasso A. Okoudjou, Luke G. Rogers, and Alexander Teplyaev, editors, *From Classical Analysis to Analysis on Fractals: A Tribute to Robert Strichartz*, volume 2 of *Applied and Numerical Harmonic Analysis*. Birkhäuser, Boston, in press, 2024. URL: https://hal.science/hal-03797595v2.

[DL24b] Claire David and Michel L. Lapidus. From Weierstrass to Riemann: The Frobenius pass – When fractal flows come into play with zeta functions. In John Friedlander, Carl Pomerance, and Michael Th. Rassias, editors, *Essays in Analytic Number Theory – in Honor of Helmut Maier's 70^{th} Birthday*. Springer Nature, Cham, in press, 2024. URL: https://hal.sorbonne-universite.fr/hal-04614665.

[DL24c] Claire David and Michel L. Lapidus. Weierstrass fractal drums - II - Towards a fractal cohomology. *Mathematische Zeitschrift*, 308(2), 2024. URL: https://hal.science/hal-03758820.

[DL25a] Claire David and Michel L. Lapidus. Iterated fractal drums ~ Some new perspectives: Polyhedral measures, atomic decompositions and Morse theory. In Hafedh Herichi, Maria Rosaria Lancia, Therese-Basa Landry, Anna Rozanova-Pierrat, and Steffen Winter, editors, *Fractal Geometry in Pure and Applied Mathematics*, volume 828 of *Contemporary Mathematics*, pages 61–130. Amer. Math. Soc., [Providence], RI, 2025. URL: https://hal.sorbonne-universite.fr/hal-03946104v3.

[DL25b] Claire David and Michel L. Lapidus. Polyhedral neighborhoods vs tubular neighborhoods: New insights for fractal zeta functions. *The Ramanujan Journal*, 67(73), 2025. URL: https://rdcu.be/en4MM.

[DL25c] Claire David and Michel L. Lapidus. Revisiting microlocal analysis: A bridge between fractal cohomology and classical function spaces. *Asymptotic Analysis, in press*, 2025.

[DL25d] Claire David and Michel L. Lapidus. Weierstrass fractal drums - I - A glimpse of complex dimensions. *Advances in Mathematics*, 481:110545, 2025. URL: https://hal.sorbonne-universite.fr/hal-03642326.

[DRSV17] Bertrand Duplantier, Rémi Rhodes, Scott Sheffield, and Vincent Vargas. Log-correlated Gaussian fields: an overview. In *Geometry, Analysis and Probability*, volume 310 of *Progr. Math.*, pages 191–216. Birkhäuser/Springer, Cham, 2017. URL: https://doi.org/10.1007/978-3-319-49638-2_9.

[Dup89] Bertrand Duplantier. *Fractal critical phenomena in two dimensions and conformal invariance*, pages 83–121. Springer US, Boston, MA, 1989. URL: https://doi.org/10.1007/978-1-4899-3499-4_4.

[Dup04] Bertrand Duplantier. Conformal fractal geometry & boundary quantum gravity. In M. L. Lapidus and M. van Frankenhuijsen, editors, *Fractal Geometry and Applications: a Jubilee of Benoît Mandelbrot, Part 2*, volume 72, Part 2 of *Proc. Sympos. Pure Math.*, pages 365–482. Amer. Math. Soc., Providence, RI, 2004. URL: https://doi.org/10.1090/pspum/072.2/2112128.

[Fal14] Kenneth Falconer. *Fractal geometry*. John Wiley & Sons, Ltd., Chichester, third edition, 2014. Mathematical foundations and applications.

[GM05] John B. Garnett and Donald E. Marshall. *Harmonic Measure*, volume 2 of *New Mathematical Monographs*. Cambridge University Press, Cambridge, 2005.

[Har16] Godfrey Harold Hardy. Weierstrass's Non-Differentiable Function. *Transactions of the American Mathematical Society*, 17(3):301–325, 1916. URL: https://www.ams.org/journals/tran/1916-017-03/S0002-9947-1916-1501044-1/S0002-9947-1916-1501044-1.pdf.

[Hor18] David Nielsen Horton. *Analysis of Weierstrass Function and its effect on Loewner Hulls*. Ph. D. Dissertation, University of Tennessee, 2018. URL: https://trace.tennessee.edu/cgi/viewcontent.cgi?article=8465&context=utk_graddiss.

[Kel17] Gerhard Keller. A simpler proof for the dimension of the graph of the classical Weierstrass function. *Annales de l'Institut Henri Poincaré – Probabilités et Statistiques*, 53(1):169–181, 2017.

[KMPY84] James L. Kaplan, John Mallet-Paret, and James A. Yorke. The Lyapunov dimension of a nowhere differentiable attracting torus. *Ergodic Theory and Dynamical Systems*, 4:261–281, 1984.

[Lap19] Michel L. Lapidus. An overview of complex fractal dimensions: From fractal strings to fractal drums, and back. In R. G. Niemeyer, E. P. J. Pearse, J. A. Rock, and T. Samuel, editors, *Horizons of Fractal Geometry and Complex Dimensions*, volume 731 of *Contemporary Mathematics*, pages 143–265. American Mathematical Society, Providence, RI, 2019. URL: https://arxiv.org/abs/1803.10399.

[Law05] Gregory F. Lawler. *Conformally Invariant Processes in the Plane*, volume 114 of *Mathematical Surveys and Monographs*. American Mathematical Society, Providence, RI, 2005. URL: https://doi.org/10.1090/surv/114.

[LG14] Jean-François Le Gall. Random geometry on the sphere. In *Proceedings of the International Congress of Mathematicians—Seoul 2014. Vol. 1*, pages 421–442. Kyung Moon Sa, Seoul, 2014.

[LG19] Jean-François Le Gall. Brownian geometry. *Japanese Journal of Mathematics*, 14(2):135–174, 2019. URL: https://doi.org/10.1007/s11537-019-1821-7.

[Lin05] Joan R. Lind. A sharp condition for the Loewner equation to generate slits. *Annales Academiæ Scientiarum Fennicæ. Mathematica*, 30(1):143–158, 2005.

[LR17] Joan Lind and Jessica Robins. Loewner deformations driven by the Weierstrass function. *Involve. A Journal of Mathematics*, 10(1):151–164, 2017. URL: https://msp.org/involve/2017/10-1/involve-v10-n1-p10-s.pdf.

[LR25] Michel L. Lapidus and Goran Radunović. *An Invitation to Fractal Geometry: Fractal Dimensions, Self-Similarity and Fractal Curves*. Graduate Studies in Mathematics. American Mathematical Society, Rhode Island, 2025.

[LRŽ17] Michel L. Lapidus, Goran Radunović, and Darko Žubrinić. *Fractal Zeta Functions and Fractal Drums: Higher-Dimensional Theory of Complex Dimensions*. Springer Monographs in Mathematics. Springer, New York, 2017.

[LSW01] Gregory F. Lawler, Oded Schramm, and Wendelin Werner. The dimension of the planar Brownian frontier is 4/3. *Math. Res. Lett.*, 8(4):401–411, 2001. URL: https://doi.org/10.4310/MRL.2001.v8.n4.a1.

[LvF00] Michel L. Lapidus and Machiel van Frankenhuijsen. *Fractal Geometry and Number Theory: Complex Dimensions of Fractal Strings and Zeros of Zeta Functions*. Birkhäuser Boston, Inc., Boston, MA, 2000.

[LvF13] Michel L. Lapidus and Machiel van Frankenhuijsen. *Fractal Geometry, Complex Dimensions and Zeta Functions: Geometry and Spectra of Fractal Strings*. Springer Monographs in Mathematics. Springer, New York, second revised and enlarged edition (of the 2006 edition), 2013.

[Mak98] Nilokai G. Makarov. Fine structure of harmonic measure. *Rossiĭskaya Akademiya Nauk. Algebra i Analiz*, 10(2):1–62, 1998.

[MP10] Peter Mörters and Yuval Peres. *Brownian Motion*, volume 30 of *Cambridge Series in Statistical and Probabilistic Mathematics*. Cambridge University Press, Cambridge, 2010. With an appendix by Oded Schramm and Wendelin Werner. URL: `https://doi.org/10.1017/CBO9780511750489`.

[PW97] Yakov Pesin and Howard Weiss. The multifractal analysis of Gibbs measures: motivation, mathematical foundation, and examples. *Chaos. An Interdisciplinary Journal of Nonlinear Science*, 7(1):89–106, 1997. URL: `https://doi.org/10.1063/1.166242`.

[RS05] Steffen Rohde and Oded Schramm. Basic properties of SLE. *Annals of Mathematics. Second Series*, 161(2):883–924, 2005. URL: `https://doi.org/10.4007/annals.2005.161.883`.

[Sch00] Oded Schramm. Scaling limits of loop-erased random walks and uniform spanning trees. *Israel J. Math.*, 118:221–288, 2000. URL: `https://doi.org/10.1007/BF02803524`.

[She18] Weixiao Shen. Hausdorff dimension of the graphs of the classical Weierstrass functions. *Mathematische Zeitschrift*, 289:223–266, 2018.

[SW01] Stanislav Smirnov and Wendelin Werner. Critical exponents for two-dimensional percolation. *Math. Res. Lett.*, 8(5-6):729–744, 2001. URL: `https://doi.org/10.4310/MRL.2001.v8.n6.a4`.

[Tit39] Edward Charles Titschmarsh. *The Theory of Functions*. Oxford University Press, second edition, 1939.

[Tra15] Huy Tran. Convergence of an algorithm simulating Loewner curves. *Annales Academiæ Scientiarum Fennicæ. Mathematica*, 40(2):601–616, 2015. URL: `https://doi.org/10.5186/aasfm.2015.4037`.

[Wei75] Karl Weierstrass. Über continuirliche Funktionen eines reellen Arguments, die für keinen Werth des letzteren einen bestimmten Differential quotienten besitzen. *Journal für die reine und angewandte Mathematik*, 79:29–31, 1875.

[Wer04] Wendelin Werner. Random planar curves and Schramm-Loewner evolutions. In *Lectures on Probability Theory and Statistics*, volume 1840 of *Lecture Notes in Math.*, pages 107–195. Springer, Berlin, 2004. URL: `https://doi.org/10.1007/978-3-540-39982-7_2`.